



Spiral Waves in the Heart

Durham University, Mathematical Sciences

PEARCE, Jex Thomas

April 2025

Abstract

This report examines the formation and dynamics of spiral waves in cardiac tissue using the FitzHugh-Nagumo model. Beginning with deterministic ordinary differential equations, then progressing to partial differential equations, we seek to model wave propagation and interactions representing cardiac heart cells. Biological and clinical representations are the core focus of this report, incorporating stochasticity through Stochastic Differential Equations, by representing natural electrolyte fluctuations in cardiac electrical activity. This research also investigates how varying levels of noise correspond to different cardiac conditions and analyzes the role of fibrotic tissue in arrhythmia formation. Throughout, we demonstrate how the FitzHugh-Nagumo framework effectively bridges mathematical modeling with biological representation, providing numerous examples of the interesting relationship between deterministic dynamics and statistical variability in cardiac function.

This piece of work is a result of my own work and I have complied with the Department's guidance on multiple submission and on the use of AI tools. Material from the work of others not involved in the project has been acknowledged, quotations and paraphrases suitably indicated, and all uses of AI tools have been declared.

Contents

1	Introduction	1
1.1	But what is a healthy heart?	3
1.1.1	Why Are Spiral Waves Dangerous?	4
1.1.2	Modeling Normal Heart Behavior	5
2	Modelling The FitzHugh-Nagumo	6
2.1	Historical Context and Application to Spiral Waves	6
2.1.1	Simplified FHN Equation and Variable Definition:	6
2.2	Mathematically Modeling The FitzHugh-Nagumo	7
2.3	Modelling The FitzHugh-Nagumo PDE	10
2.4	Modeling Spiral Waves in 2D	13
2.5	Updates to the Iterative Loop and Boundary Conditions	14
2.6	Final Output of Model:	14
2.7	Applying a Defibrillator Shock	15
3	Dead Cell Induced Spiral Formation & Period Analysis	16
3.0.1	Incorporating Dead Cells	16
3.1	Analyzing the Period of the 2D Spiral Waves	18
3.1.1	Calculating the Average Period	19
3.1.2	Measuring the Period of the Dead Cell model:	20
3.2	Electrode Probes: Locating the Spiral Source with Triangulation	21
3.2.1	Applying Targeted Defibrillation with Probe Prediction	24
4	Representing Cardiac Diseases in the Heart with Electrolyte Stochasticity	29
4.1	Electrolytes and Cardiac Wave Propagation: The Basics	29
4.2	Modeling Electrolyte Imbalances as a Source of Cardiac Stochasticity	30
4.3	The Additive White Noise Model	31
4.4	The Coloured Noise Model: The Ornstein-Uhlenbeck Process	33
4.4.1	Mathematical Definition	33
4.4.2	Low Parameter Values: Normal Heart Behavior	34
4.4.3	Moderate Parameter Values: Tachycardia-Like Behavior	35
4.4.4	High Parameter Values: Fibrillation-Like Dynamics	36
5	Fibrosis: Regional Tissue Variation	38
5.1	Varying the Region Size and Severity of Fibrosis Damage	40
5.1.1	Concentrated High levels of Damage: Representing Automatic Foci	40
5.2	Fibrotic Region Size Analysis:	41
6	Quantifying Vulnerability: MRT Spiral Formation Analysis of Fibroticity:	43
6.1	MRT for Spiral Formation in Varying Sizes of Fibrotic Damage	43
6.1.1	Defining Spiral Wave Detection	43
6.1.2	Spiral Tip Detection Algorithm	44
6.1.3	MRT Result and Heatmap:	45
6.1.4	Parameter Influence Analysis:	46
6.2	MRT for Spiral Formation in Varying Sizes of Fibrotic Damage	47
6.2.1	Biological Research on Fibrotic Size:	47
6.3	Mathematical MRT Setup for Size Variation:	48
6.3.1	Spiral Formation Time V. Damaged Region Size Graph and Analysis	49
6.3.2	Quadratic Trend Analysis	50
6.3.3	A Conclusive Written Analysis of Spiral Formation Time and Damaged Region Size	51
7	Conclusion	52

1 Introduction

The human heart is a remarkable organ, whose primary function is to pump blood rhythmically and efficiently throughout the body. This rhythmic contraction is controlled by an electrical signaling system that propagates through the heart's tissue, ensuring that each heartbeat is precisely timed. In a healthy heart, these electrical waves follow well-defined pathways, depending on the precise balance of electrolytes, that maintain the heart's regular rhythm. However, under certain abnormal conditions, this orderly rhythm can be disrupted, leading to the emergence of self-sustaining spiral waves in the heart. These spirals then 're-enter' and circulate continuously around the organ that when combined with the heart's natural periodic rhythm can be associated with life-threatening arrhythmias, which claim over 300,000 lives in the USA annually.

The most important method for analyzing these cardiac arrhythmia-causing spirals is undoubtedly with mathematical modeling. The FitzHugh-Nagumo (FHN) equation, originally developed for neural excitability in the early 1960s, has proven particularly effective for studying cardiac electrodynamics. Its simplified representation of excitable media offers a powerful approach for investigating wave propagation, including the formation and behavior of spiral waves in cardiac tissue.

In this dissertation, a foundation of healthy cardiac electrical activity will be established, followed by an extensive exploration of spiral wave phenomena and their detrimental impact on cardiac function. This is achieved first with ordinary differential equations to understand the fundamental dynamics, and then progressing to partial differential equations that will incorporate spatial diffusion, a key factor in representing the spread of electrical signals across cardiac tissue.

A key focus of this section will be the dead cell model, which represents one of the most common mechanisms of spiral formation in the heart. In this model, non-excitatory regions will force normal waves to bend and wrap around obstacles, creating the conditions for spiral generation. A potential treatment method will also be briefly examined, using probe placement for spiral source detection via period analysis followed by a targeted defibrillation technique.

Beyond these deterministic models, focus will then be shifted to the role of randomness in cardiac dynamics. Nature is never perfect, and heart cells are no exception. Their behavior is heavily controlled by various stochastic processes, the most prominent being electrolyte dynamics, where fluctuations in ion channels and concentration gradients can affect cardiac electrical activity immensely. By introducing the Ornstein-Uhlenbeck process, a more realistic model that utilizes time-dependent noise, it will allow us to create a biologically realistic representation of how cardiac cells behave. This stochastic framework will let us explore how different levels of stochasticity in electrolyte concentrations can contribute and represent cardiac arrhythmias. A further dive into period analysis will then be used to connect these mathematical models with clinically defined diseases and phenomena.

With our stochastic framework on realism established, Fibrosis, a 'weakened' region of the heart, will also be examined. Unlike dead cells, fibrosis is characterized by regions of weakened but still excitable tissue, and it is a common cardiac condition many develop after heart attacks or with age. An analysis on how fibrosis creates the perfect storm of conditions for potential arrhythmias to arise will also be conducted, using the FitzHugh-Nagumo model with altered parameters. A major focus will also be developing a Mean Response Time (MRT) methodology to quantify how quickly spirals could form under different sizes and severity of the fibrotic region in a physiologically feasible simulation time. We will then seek to establish a quantifiable relationship between the severity of the damaged region, the size,

and how long it takes for a spiral to form in the parameter space.

Throughout this work, the main goal will be to bridge pure mathematics with biological reality. We shall achieve this by seeking the creation of three key contributions: first, demonstrating how deterministic mechanisms, such as dead cells, create spiral waves; second, showing how electrolyte fluctuations, modeled through the Ornstein-Uhlenbeck process, influence arrhythmia formation; and third, utilizing the latter to develop a Mean Response Time methodology for quantifying spiral formation in fibrotic tissue. Additionally, a key objective will be to verify the efficacy of the FitzHugh-Nagumo model in representing wave propagation in excitable media, particularly in its application to cardiac dynamics. In summary, this research will provide information about the complex relationship between deterministic cardiac dynamics and realistic inherent biological behavior, offering a foundation for future work on more realistic heart models.

1.1 But what is a healthy heart?

Electrical activity in the heart is highly organized and complicated, and one could write up an extensive report on the topic. While a deep dive into anatomy will not be the focus of this report, an aforementioned bridge to biological reality will still be conducted, so a descriptive simplification of the process will be required.

Sinoatrial (SA) Node - The Heart's Natural Pacemaker The *sinoatrial (SA) node*, located in the top left atrium, generates the initial electrical impulse. This impulse is often called the "*pacemaker signal*" and occurs at regular periodic intervals. The SA nodes rhythmic firing sets the pace for the entire heart, controlling its overall rate and rhythm.

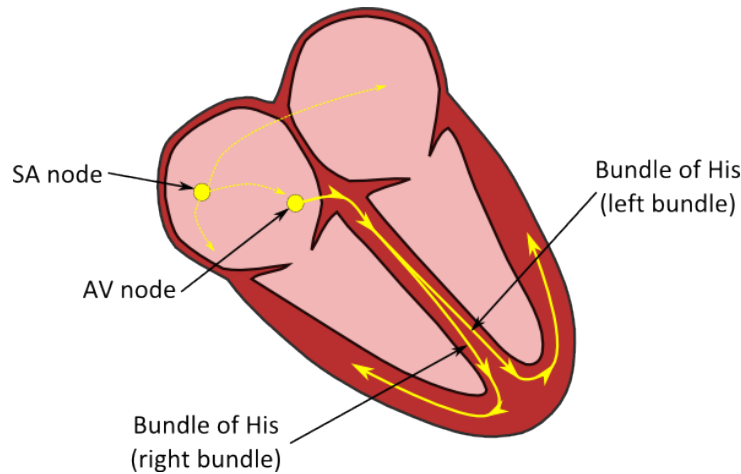


Figure 1: A simplified model of the Sinoatrial node and its role in electrical heart wave propagation [22].

The SA node generates electric action potentials which then spread across both the right and left atria, facilitated by electrolytes (sodium, potassium, and calcium ions), which then trigger their contraction, pushing blood into the ventricles. In this report, these electric action potentials will be represented mathematically as visible waves propagating downward through the organ. This electrical impulse then reaches the atrioventricular (AV) node, the only pathway for action potentials to enter the ventricles. The atria and ventricles are electrically separated by the cardiac skeleton, a connective tissue framework which also provides structural support for the heart valves. From the AV node, electrical signals travel down the bundle of His, a conduction pathway that distributes impulses throughout the ventricles, causing ventricular contraction and completing a full cardiac cycle - what we recognize as a single heartbeat.

The crux of the project: Pathological Cardiac Dynamics

When electrical wavefronts propagating through the atria encounter disruptions, they can fragment and reorganize into spiral waves.

These disruptions can arise from various factors including dead cells, fibrotic scarring, or varying electrolyte imbalances. Once formed, spiral waves create self-sustaining rotors that override the SA node's pacemaker function, forcing the heart to beat at significantly higher frequencies. This report will examine the mechanisms of spiral wave formation through mathematical modeling, analyzing the dynamics of cardiac arrhythmias from these aforementioned factors.

1.1.1 Why Are Spiral Waves Dangerous?

When spiral waves form, they disrupt the healthy heartbeat in many harmful ways. A few examples:

1. **Rapid, Chaotic Beating:** Instead of the Sinoatrial node's steady 60-80 beats per minute, spiral waves can force regions of the heart to contract much faster, with more blood being pushed into the ventricles at a faster rate.
2. **Self-Sustaining Nature:** Unlike normal heartbeats that require the Sinoatrial node's signal, spiral waves can self-perpetuate. They create their own rotating pattern of activation that can continue indefinitely without external input, making them particularly dangerous.

The end result is that the heart becomes more like a quivering mass than an efficient pump. This condition can result in insufficient blood flow to vital organs. In the ventricles (lower chambers), this is particularly dangerous and can be fatal if not treated, as the heart is no longer effectively pumping blood to the rest of the body.

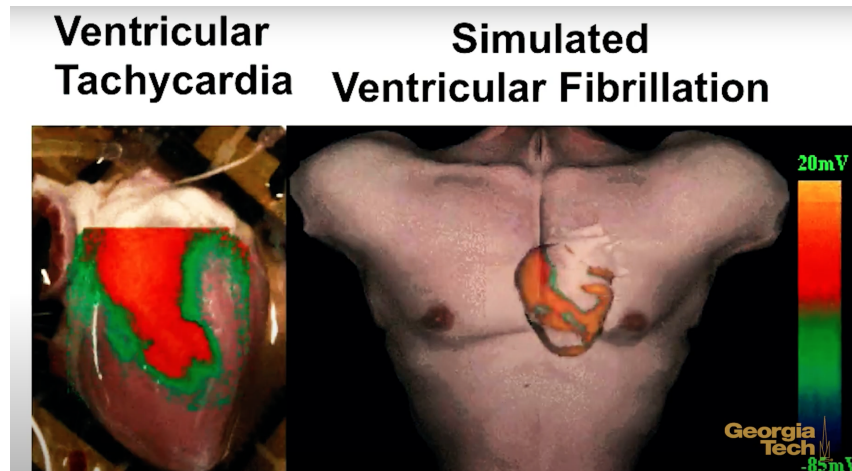


Figure 2: A 3D visualization by Georgia Tech conveying this dangerous anomaly [23]. The spiral overpowers the heart's natural heartbeat and dominates the dynamics of the organ. Unless otherwise stated, all images and animations forward have been created by myself with Python and other mathematical modeling techniques.

The Discovery of Spiral Waves in the Heart

The concept of spiral waves in cardiac tissue dates back to the mid-20th century, when researchers first analyzed and explored how electrical wave fronts propagate in excitable systems. In 1946, after conducting numerous cardiac experiments, Wiener & Rosenblueth proposed a theoretical model for

reentrant, self-sustaining waves in heart tissue, laying the foundations for understanding spiral wave formation.

By the 1970s and 1980s, experimental studies using optical mapping techniques began confirming these theoretical predictions. In 1991, Davidenko et al. generated visual proof of spiral waves in cardiac tissue, showing how reentrant excitation could self-sustain. He also analyzed how these waves could destabilize normal heart rhythms, and linked these spiral waves to life-threatening arrhythmias (cardiac diseases) [37].

1.1.2 Modeling Normal Heart Behavior

The heart, being a three-dimensional organ, is computationally challenging to model. To allow computer simulations to be performed with the computing capabilities available with a standard laptop, I will simplify the computational complexity by using a two-dimensional vertical slice of the heart. This slice will then represent the electrical waves propagating through that specific section.

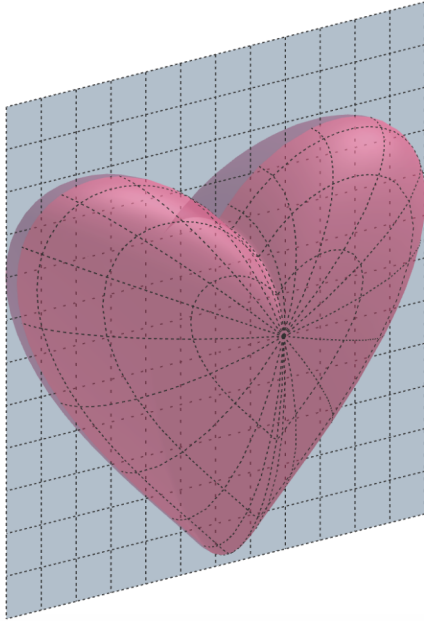


Figure 3: A 2D slice of a 3D cartoon heart

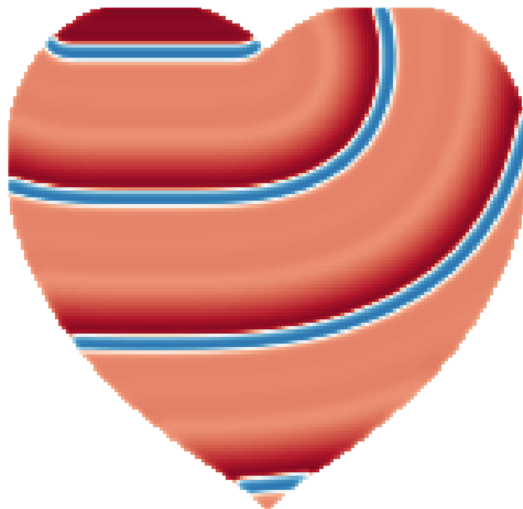


Figure 4: The healthy heartbeat waves propagate downward from the top left corner of the model at a rate of 60bpm.

For a better idea of what this looks like visually, here is the animation of the normal heart model animated over time: [Click Here:](#)

This animation represents the normal behavior of a healthy heart at the average 60bpm, with no disruptions such as perturbations, dead cell regions, or damaged fibrotic areas. From this point onward, the focus of this project will shift to exploring how various external and internal influences can disrupt this normal behavior, leading to phenomena such as spiral waves in the heart.

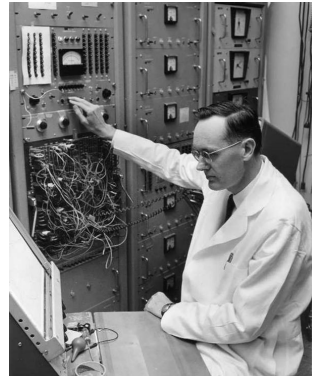
To model such phenomena mathematically, we need a framework that can capture both the normal electrical behavior of heart tissue and how it can become disrupted. This must represent how electrical waves propagate and move through cardiac cells and how spirals can form under certain conditions. At the core of this exploration lies the FitzHugh-Nagumo model, a mathematical framework that enables us to simulate and analyze these disruptions and their effects on cardiac dynamics.

2 Modelling The FitzHugh-Nagumo

2.1 Historical Context and Application to Spiral Waves

Created by Richard FitzHugh and Jinichi Nagumo, the FitzHugh-Nagumo model was first proposed in the early 1960s as a simplified alternative to the Hodgkin-Huxley equations for neural excitability. While originally developed to progress work on neural systems, the FHN equation has been recently adapted to model spiral wave phenomena in the heart. Its advantage is how the model's simplicity allows us to analyze spiral wave formation with limited computational requirements.

Figure 5: Scientist Richard FitzHugh utilizing an analog computer to build a representation of electrical behavior in neuron cells [24].



2.1.1 Simplified FHN Equation and Variable Definition:

$$\frac{du}{dt} = \frac{1}{\epsilon} \left(u - \frac{1}{3}(u)^3 - v \right), \quad (1)$$

$$\frac{dv}{dt} = \epsilon(u + \beta - \gamma v). \quad (2)$$

The FitzHugh-Nagumo (FHN) equation focuses on two state variables: the excitatory variable u , and the recovery variable v . These variables represent the electrical excitatory potential, u , and the recovery of the system, v .

ϵ , β , and γ : The Three Important Parameters of the FitzHugh-Nagumo Equations:

The FHN equation has three important parameters, ϵ , β , and γ , each of them influencing the system:

- ϵ : Controls the timescale separation between the fast excitation of u and the slower recovery dynamics of v . A smaller ϵ leads to a higher change of u compared to v due to a slower recovery phase.
- β : Determines the threshold for excitation. A lower β means that it's easier for the system (ex. a heart cell) to transition from rest to excited. The higher it is the harder.
- γ : Influencing how the recovery variable v dampens the excitatory behavior.

Scientists typically choose $\epsilon = 0.3$, $\beta = 0.7$, and $\gamma = 0.5$ for the FHN equation, as these values produce spirals with minimal tip movement that can be analyzed effectively. In biological terms, β represents the activation threshold potential of cardiac cells, ϵ controls the excitation-recovery timescale separation, and γ determines the recovery rate after excitation. Later sections will go more in depth on the cardiac biological connections these parameters have, and how adjusting them can affect the systems dynamics.

2.2 Mathematically Modeling The FitzHugh-Nagumo

Starting with an ordinary differential equation (ODE), the FHN model is defined as a system of coupled ODEs describing the dynamics of two state variables, u - (excitatory variable) and v (recovery variable).

These ODEs represent the rate of change of these variables over time and they are a good representation of the underlying processes driving excitability and oscillations in heart tissue. While spatial coordinates (locations) are not a factor here, we can still determine equilibrium points, study the stability of the system, and explore how perturbations evolve. We will begin with the steps necessary to construct a plot of this ODE system over time.

Finding the Equilibrium Points:

Nullclines are curves in the phase plane where the derivative of a variable in a dynamical system equals zero, representing the system's fixed points. Spiral wave behavior often occurs near these Nullcline fixed points where the dynamics are not purely stable or unstable but oscillatory.

1. **u -nullcline:** The curve where $\frac{du}{dt} = 0$ in equation (1).

2. **v -nullcline:** The curve where $\frac{dv}{dt} = 0$ in equation (2).

The intersection points of the u - and v -nullclines correspond to the equilibrium points of the system, where the system is stationary ($\frac{du}{dt} = 0$ and $\frac{dv}{dt} = 0$).

$$0 = \frac{1}{\epsilon} \left(u^* - \frac{1}{3}(u^*)^3 - v^* \right), \quad (3)$$

$$0 = \epsilon(u^* + \beta - \gamma v^*). \quad (4)$$

With given parameters $\epsilon = 0.3$, $\beta = 0.7$, and $\gamma = 0.5$. Curiosity as to why those values of $\epsilon = 0.3$, $\beta = 0.7$, $\gamma = 0.5$ have been chosen may arise. Researchers often choose a range of plausible values from the literature. For the FitzHugh-Nagumo model, the parameter values above. are standard because they produce a balance of timescales and interaction strengths known to generate realistic dynamics.

Solving equation (4) for v^* :

$$u^* + 0.7 - 0.5v^* = 0 \Rightarrow v^* = 2u^* + 1.4.$$

Substitute v^* into equation (3):

$$u^* - \frac{1}{3}(u^*)^3 - (2u^* + 1.4) = 0 \Rightarrow (u^*)^3 + 3u^* + 4.2 = 0.$$

Newton-Raphson Method: For the cubic equation $(u^*)^3 + 3u^* + 4.2 = 0$, we apply Newton-Raphson iteration: $u_{n+1} = u_n - \frac{f(u_n)}{f'(u_n)}$, where $f(u) = u^3 + 3u + 4.2$ and $f'(u) = 3u^2 + 3$.

Starting with $u_0 = -1.0$, after two iterations: $u_1 = -1 - \frac{0.2}{6} \approx -1.033$ $u_2 = -1.033 - \frac{-0.0023}{6.203} \approx -1.033$

The solution converges to $u^* \approx -1.033$, yielding $(u^*, v^*) \approx (-1.033, -0.666)$.

Final Equilibrium Point:

$$(u^*, v^*) \approx (-1.0328, -0.6658)$$

We can verify this by substituting $u^* = -1.0328$ and $v^* = -0.6658$ back into the original equations (3) and (4) to get 0 for both.

The Nullcline Equations:

After setting $\frac{du}{dt} = 0$ and $\frac{dv}{dt} = 0$ as above, we can rearrange the terms in (3) and (4) to get simplified, concise versions of:

- The u -nullcline (3) ($\frac{du}{dt} = 0$). This is the **nonlinear nullcline**, represented as a cubic curve in the u - v plane below.

$$v = u - \frac{u^3}{3}. \quad (5)$$

- The v -nullcline (4) ($\frac{dv}{dt} = 0$). This is the **linear nullcline**, represented as a straight line in the u - v plane.

$$v = \frac{u + \beta}{\gamma}. \quad (6)$$

Starting Initial Conditions:

Our starting initial conditions are taken to be close to the equilibrium point:

$$(u, v) = (u^* + 0.29, v^*) \text{ for } (u^*, v^*) \approx (-1.0328, -0.6658)$$

The value of 0.29 has been added to the u^* value to ensure motion successfully begins and we can observe the system's behavior. Starting the simulation exactly at (u^*, v^*) would result in no motion in the phase plane since the system would remain at rest.

1: Defining the First Variables: Starting parameters and nullclines code:

```

1 epsilon = 0.3
2 beta = 0.7
3 gam = 0.5
4 ustardot = -1.032789870 # The fixed points found before.
5 vstardot = -0.6655797400
6 # Initial conditions and Nullclines
7 u = ustardot + 0.29
8 v = vstardot
9 nonlinearline = u - u**3 / 3.0 # du/dt = 0 (nonlinear)
10 linearline = (u + beta) / gam # dv/dt = 0 (linear)

```

Numerical Time Evolution of the System:

To track how the FHN (Fitzhugh-Nagumo) system evolves over **time**, we use Euler's method, a simple numerical integration technique. Starting with the initial conditions $(u_0, v_0) = (u^* + 0.29, v^*)$, the equations for u and v are updated at each step using the following formulas:

Finite Increment Approximation (Euler's Method): The derivative $\frac{du}{dt}$ tells how u changes per unit of time. Over a small time interval Δt , which we will call $\Delta t = 0.01$, the change in u and v is approximately:

$$u_{t+\Delta t} \approx u_t + \Delta t \cdot \frac{du}{dt}, \quad v_{t+\Delta t} \approx v_t + \Delta t \cdot \frac{dv}{dt}.$$

Thus, substituting in our previous equations for $\frac{du}{dt}$ and $\frac{dv}{dt}$:

$$u_{t+\Delta t} = u_t + \Delta t \cdot \frac{1}{\epsilon} \left(u_t - \frac{u_t^3}{3} - v_t \right), \quad v_{t+\Delta t} = v_t + \Delta t \cdot \epsilon (u_t + \beta - \gamma v_t). \quad (7)$$

- Time step size: $\Delta t = 0.01$, and System parameters: $\epsilon = 0.3, \beta = 0.7, \gamma = 0.5$

Iterating over a python simulation in the (u,v) phase plane, starting from the perturbed initial conditions of $(u_0, v_0) = (u^* + 0.29, v^*)$, we can find a good representation of what this system will look like overtime.

Full Code and Output of the Static FHN ODE

Full code for the FHN ODE Phase Plane model below that represents the trajectory of the dynamics of the system, and the Time Evolution model: [phaseplanecode.txt](#), [timeevolutioncode.txt](#).

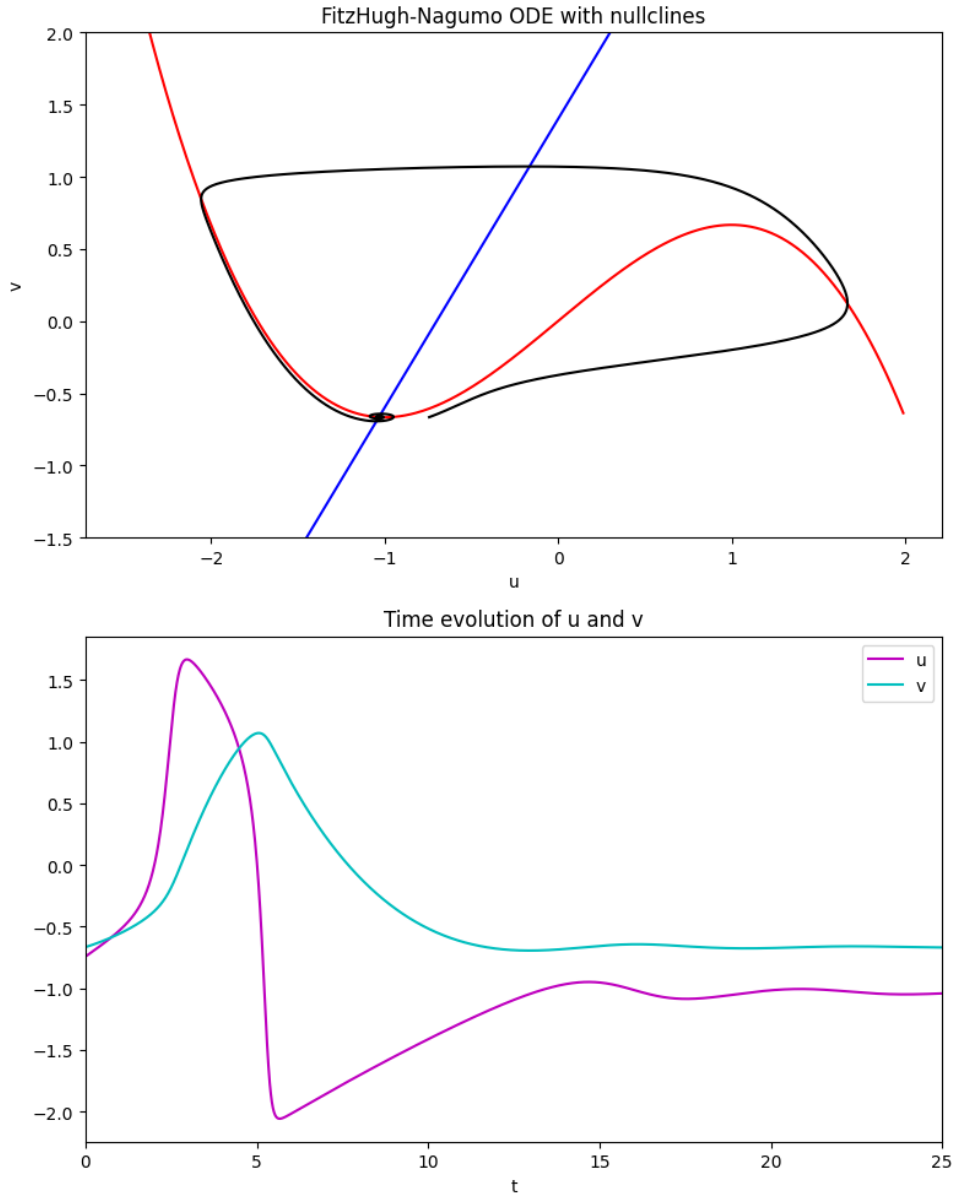


Figure 5: The FHN ODE Phase Plane and Time Evolution models. Time Evolution with time units 0 to 25, in 8 seconds of animation time corresponds roughly to 3 time units per second in this model.

Animated Model and an Analysis: To see the ODE's Phase Plane Evolution animated visually: [Click Here](#):. To see the ODE's Time Evolution animated visually: [Click Here](#):. The red u -nullcline (5), and the blue v -nullcline (6), equilibria intersect at approximately $(-1.0328, -0.6658)$ as expected. Examine the system's oscillatory and stabilizing behavior with the black trajectory line, which illustrates the system's time evolution. This spirals around and eventually stabilizes near the equilibrium point.

2.3 Modelling The FitzHugh-Nagumo PDE

While ODEs excel in representing temporal, time based behavior, spatial propagation requires partial differential equations to model how electrical signals spread across cardiac tissue. By incorporating spatial diffusion, this model will allow us to simulate how perturbations evolve over space and time.

Defining the Spatial Domain

The first step in solving the PDE is defining a discrete spatial grid area to represent the system. The spatial domain is set up as follows:

1. Length of the Domain (L):

- While this will vary in future models, the total length of the domain here is $L = 100$, spanning from $x = -50$ to $x = 50$.

2. Number of Grid Points (m):

- A total of 201 grid points ($m = 201$) is chosen. This 'odd' choice of a number is so that the center of the grid ($x = 0$) aligns with a discrete grid point and not in between two.

3. Spatial Step Size (Δx):

- The distance between adjacent grid points is calculated as $\Delta x = 0.25$, providing a fine resolution for accurate numerical differentiation.

4. Grid Array (x):

- The grid points are represented by a numpy array, $x = np.linspace(-50, 50, 201)$, allowing the system to evaluate the u and v -values at each point in space.

2: Spatial domain code:

```

1 L = 100.0 #length
2 m = 201
3 dx = 0.5
4 x = np.linspace(-50, 50, m) #spatial grid points -50 to 50
5 dt = 0.01

```

A Gaussian Perturbation

A perturbation is now needed here, since the points are all initially at equilibrium. Using a *Gaussian Perturbation*, it will affect the excitatory u -variable, representing a localized disturbance at $t=0$. The functional form of the 1D Gaussian perturbation is mathematically expressed as:

$$G(x) = a \exp(-bx^2) \quad (8)$$

where $a = 0.5$ is the amplitude controlling the strength of the perturbation in this model, and $b = 0.05$ will determine the width. A larger b makes the perturbation narrower and more concentrated, while a smaller b makes it wider and more spread out. Here, $G(x)$ will be $u(x, t = 0)$, where the excitatory u is perturbed by a Gaussian centered at $x = 0$:

$$u(x, t = 0) = u^* + ae^{-bx^2}, \quad (9)$$

with u^* as the equilibrium value of u , and ae^{-bx^2} representing the localized perturbation.

The exclusion of v is no error, as applying the Gaussian Perturbation on the recovery variable v is not required to generate a traveling wave, since rotational symmetry is not needed yet. v will be set to v^* at $t = 0$.

3: Gaussian Perturbation code:

```

1 a = 0.5
2 b = 0.05
3 u = ustard + a * np.exp(-b * x**2)
4 v = np.ones(m) * vstar

```

Adding the Laplacian

The core of the Partial Differential Equation. The Laplacian represents the second spatial derivative and accounts for how u diffuses across the spatial grid. This will be implemented with a numerical approximation below for the 1D PDE. It's only applied to the excitatory u variable since it needs to capture spatial interactions effectively, whereas v acts more upon the recovery, and an applied Laplacian on v would not fundamentally change the system's behavior. We can express this below with a Finite Difference Approximation, later on it will be referenced as $\nabla^2 u$.

1. Second Derivative Approximation:

$$\frac{\partial^2 u}{\partial x^2} \approx \frac{u_{i+1} - 2u_i + u_{i-1}}{\Delta x^2}.$$

Here, u_i represents the value of u at grid point i , and Δx is the spatial step size. u_{i+1} represents the value of u at the grid point 'after' i , and u_{i-1} is the one before it. Essentially this looks at the grid point before, the point it's on, and the point after divided by step size to determine how u diffuses across the grid.

```

1 d2u_dx2 = np.zeros(m) #to store second derivative
2 d2u_dx2[1:-1] = (u[2:] - 2*u[1:-1] + u[:-2]) / dx**2

```

Notice as well that the boundary points are excluded to avoid errors, as the second derivative is not well-defined there (there's no point before/after to analyze per say).

2. Time Evolution:

Like in the ODE, we will use Euler's method for time-stepping, the u - and v -values are updated at each time step:

$$u_i^{n+1} = u_i^n + \Delta t \left[\frac{1}{\epsilon} \left(u_i^n - \frac{(u_i^n)^3}{3} - v_i^n \right) + \frac{u_{i+1}^n - 2u_i^n + u_{i-1}^n}{(\Delta x)^2} \right], \quad v_i^{n+1} = v_i^n + \Delta t [\epsilon (u_i^n + \beta - \gamma v_i^n)]$$

For the explicit Euler method applied to the FitzHugh-Nagumo PDE, numerical stability requires the CFL (Courant-Friedrichs-Lowy) condition: $\Delta t \leq \frac{(\Delta x)^2}{2D}$. With our parameters $\Delta x = 0.25$, $D = 1$, this gives $\Delta t \leq 0.03125$. The choice of $\Delta t = 0.01$ satisfies this condition, ensuring numerical stability throughout the simulation.

The corresponding Python code is:

```

1 # Update interior points using Euler's method
2 u[1:-1] = u[1:-1] + dt * (ut[1:-1] + d2u_dx2[1:-1])
3 v[1:-1] = v[1:-1] + dt * vt[1:-1]

```

3. Boundary Conditions: The Laplacian does not work at the borders. But it's essential to handle them with Dirichlet boundary conditions, to enforce fixed values of u^* and v^* at the edges of the spatial grid:

```

1  u[0], u[-1] = ustar, ustar # Fixed boundary for u
2  v[0], v[-1] = vstar, vstar # Fixed boundary for v

```

Final FHN Equations:

Therefore, we can create the final Fitzhugh Nagumo PDE equations below.

$$\frac{\partial u}{\partial t} = \frac{1}{\varepsilon} \left(u - \frac{1}{3}u^3 - v \right) + \nabla^2 u, \quad \frac{\partial v}{\partial t} = \varepsilon(u + \beta - \gamma v) \quad (10)$$

Full Code, Output, and Animation Full code can be accessed here: [full1Dpdecode.txt](#).

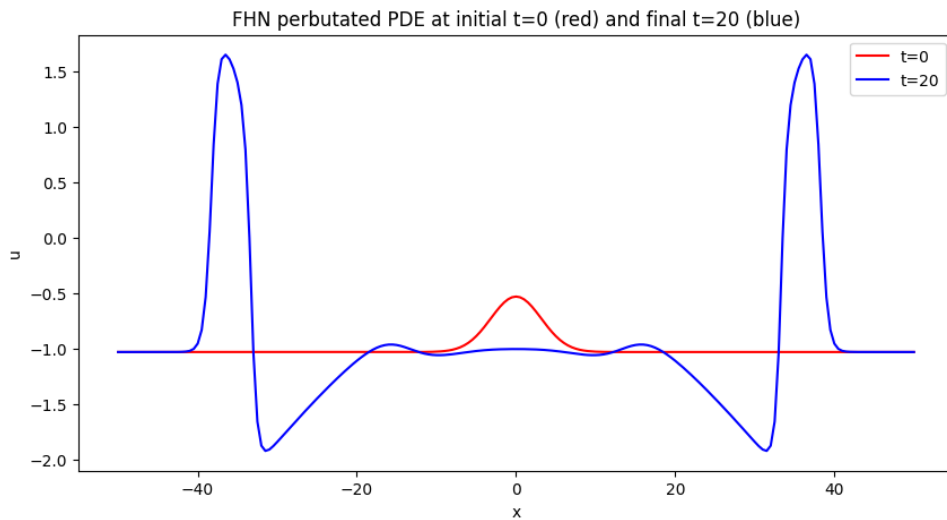


Figure 6: A still of the FHN PDE animation. The red line indicates the starting position at $t = 0$, and the blue line represents the final shape of the wave at $t = 20$. Over time, the initial localized disturbance propagates and interacts with the system's dynamics, leading to the formation of distinct spatial patterns.

To see the time evolution animated visually: [Click Here](#).

Other Relevant Models/Animations:

Restricted to Positive Spatial Points: To see this time evolution animated visually: [Click Here](#). Notice how this resembles heartbeats in a electrocardiogram (ECG or EKG) machine. **Periodic Perturbations:** [Click Here](#):

2.4 Modeling Spiral Waves in 2D

While modeling the FitzHugh-Nagumo system in one dimension provides insights into wave propagation, a 2D simulation is essential to observe the emergence and dynamics of spiral waves through a vertical slice of the heart.

Setting Up the 2D Grid

To simulate the propagation of electrical signals in two dimensions, we first define a discrete spatial grid. The grid is constructed using a square domain, where each point represents a location in the 2D medium. The spatial domain is divided into evenly spaced intervals with grid points determined by the step size resolution parameter $\Delta x = 0.25$, as it is the number of points in the space (50) divided by the number of points (201) minus 1.

The `np.linspace` function with `np.meshgrid`, will be used to form the points x points grid:

4: 2D grid setup code:

```

1 points = 201
2 dx = 0.25
3 #np.linspace('starting point', 'ending point', 'number of points'
4 x = np.linspace(0, 50, points)
5 y = np.linspace(0, 50, points)
6 X, Y = np.meshgrid(x, y)

```

The parameters for the grid are as follows:

- **Domain Size:** A square domain spanning [0, 50] in both x - and y -directions.
- **Number of Grid Points:** 201×201 , the `points` variable.
- **Spatial Step Size (Δx):** 0.25, written as `dx`

Adjusting the Gaussian Perturbation for 2D:

Unlike the 1D case, where the perturbation is applied along a single spatial axis, in the 2D model, the Gaussian perturbation needs to account for spatial variation across both dimensions. This introduces a localized disturbance that combined with all the grid points being concurrently applied with the FitzHugh-Nagumo equation, will form a spiral at the location specified. The functional form of the 2D perturbation will now be mathematically expressed as:

$$G(X, Y) = A \exp \left(- \left(\frac{X^2}{\sigma_X^2} + \frac{Y^2}{\sigma_Y^2} \right) \right) \quad (11)$$

With A amplitude as before, σ_X and σ_Y are the widths of the spread of the Gaussian perturbation in the x and y direction respectively. A larger value (ex. 100) makes the perturbation wider and more spread out, while a smaller value would make it narrower and more concentrated. The location of this disturbance can also be controlled by altering the center of X^2, Y^2 . Adding the equilibrium values of u^* and v^* to u and v , we choose:

$$u = u^* + 10 \cdot \exp \left(- \frac{(X - 10)^2}{100} \right), \quad v = v^* + 10 \cdot \exp \left(- \frac{(Y - 10)^2}{100} \right), \quad (12)$$

Where $X = 10$ and $Y = 10$, a vertical and horizontal slice intersecting in the center, is where the location of this perturbation is, with an amplitude of $A = 10$ strength. Given this expression will be defined at the start of the iterative loop, this perturbation will occur instantly at $t = 0$.

The reason this perturbation above is applied to both the u and v values is because in 2D, spiral waves require a broken symmetry or a phase difference between u and v at different spatial locations. If only u is perturbed, the system might only generate simple traveling waves rather than the necessary wave breakup that leads to spiral formation. Perturbing both u and v ensures that different regions of the domain are in different phases of excitation and recovery, a combination that is mathematically necessary for rotational spiral formation.

Thus, this mathematical technique gives us the necessary tools to choose a location for a potential spiral to form.

2.5 Updates to the Iterative Loop and Boundary Conditions

After defining the 2D grid and introducing the Gaussian perturbation, the next step involves altering the FitzHugh-Nagumo model equations over time to incorporate this new layout. A short summary of the new notation that follows:

Let $u_{i,j}^n$ represent the value of the variable u at grid point (i, j) during the time step n . The neighboring grid points are defined as follows:

$u_{i+1,j}^n$ denotes the grid point adjacent to (i, j) in the positive x-direction.

$u_{i-1,j}^n$ represents the grid point adjacent to (i, j) in the negative x-direction.

$u_{i,j+1}^n$ indicates the grid point directly above (i, j) in the positive y-direction,

$u_{i,j-1}^n$ represents the grid point directly below (i, j) in the negative y-direction.

Full equations below.

$$u_{i,j}^{n+1} = u_{i,j}^n + \Delta t \left[\frac{1}{\epsilon} \left(u_{i,j}^n - \frac{(u_{i,j}^n)^3}{3} - v_{i,j}^n \right) + \nabla^2 u_{i,j}^n \right],$$

$$v_{i,j}^{n+1} = v_{i,j}^n + \Delta t \cdot \epsilon (u_{i,j}^n + \beta - \gamma v_{i,j}^n),$$

where $\nabla^2 u_{i,j}^n$ is the discrete Laplacian operator, and since it also needs to account for the diffusion of u in both x - and y -directions here, the Laplacian $\nabla^2 u$ will now be computed as:

$$\nabla^2 u_{i,j}^n = \frac{u_{i+1,j}^n - 2u_{i,j}^n + u_{i-1,j}^n}{\Delta x^2} + \frac{u_{i,j+1}^n - 2u_{i,j}^n + u_{i,j-1}^n}{\Delta x^2}.$$

5: Code for updated FHN Equations for 2D:

```

1 ut = (u[1:-1, 1:-1] - (u[1:-1, 1:-1] ** 3)/ 3 - v[1:-1, 1:-1])
2 / epsilon
3 vt = epsilon * (u[1:-1, 1:-1] + beta - gam * v[1:-1, 1:-1])
4 u2x = (u[2:, 1:-1] - 2 * u[1:-1, 1:-1] + u[:-2, 1:-1]) /dx**2
5 u2y = (u[1:-1, 2:] - 2 * u[1:-1, 1:-1] + u[1:-1, :-2]) /dx**2
6 u2xy = u2x + u2y #adding them together as above

```

This concludes all the important mathematically relevant changes. Full code: [full2Dpdecode.txt](#).

2.6 Final Output of Model:

Here is the animation video: [Click Here](#):

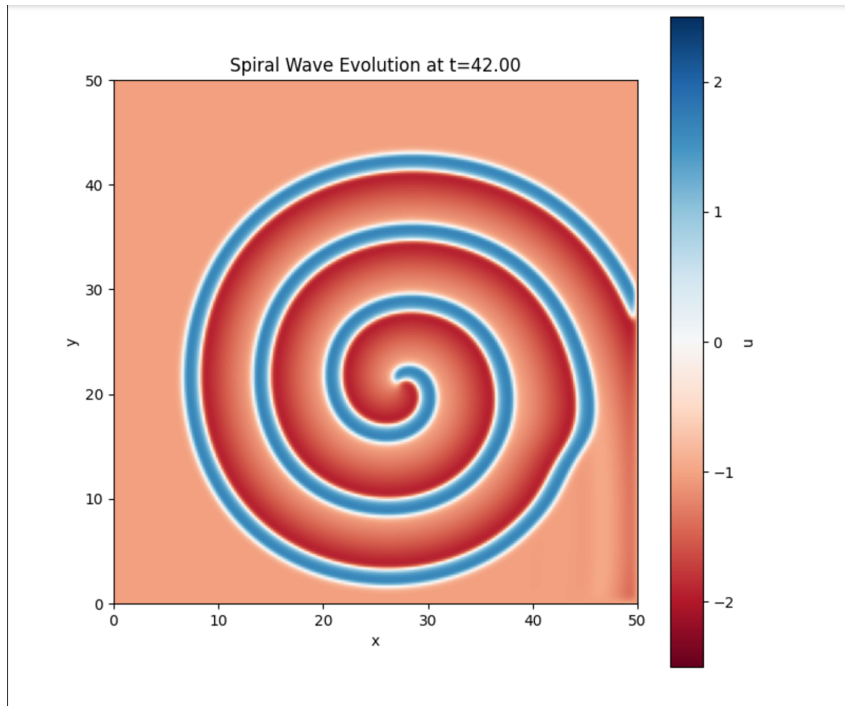


Figure 7: A Spiral forming from a Gaussian Perturbation in the established 2D grid

2.7 Applying a Defibrillator Shock

To simulate a defibrillator being applied to the entirety of the heart, we can apply a stimulation to every point's u variable at a specific time duration after the spiral has formed.

6: Code for the uniform shock

```

1 shock_time = 3000 # at what loop number to apply it
2 shock_duration = 1.0 # How long the shock lasts
3 shock_amplitude = 1.0 # Strength of the shock
4 #integrating it into the for loop
5 if shock_time <= i < shock_time + shock_duration:
6     u = u + shock_amplitude #Uniform shock across entire domain

```

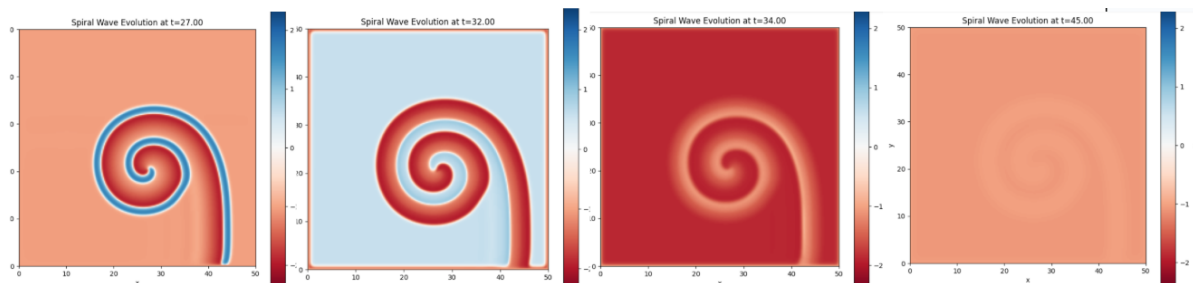


Figure 8: Evolution of the uniform shock applied to the grid. Halfway through the simulation time, the entire grid is flooded with a stimulation, representing a defibrillator. At the end of the simulation, all traces of the spiral and a potential healthy heartbeat have dissipated from the grid.

3 Dead Cell Induced Spiral Formation & Period Analysis

The propagation of electrical waves in the heart is essential for maintaining a regular rhythm. As seen back in chapter 1, a healthy heart has electric pulses originating from the top left in the sinoatrial node. However, disruptions caused by damaged cardiac tissue, such as dead cells, can lead to formations of their own spirals upon contact with the normal electric heart pulses. By introducing a region of non-conductive "dead cells," the periodic waves are disrupted, resulting in the formation of spirals. These spirals can then interfere with the normal periodic heartbeat waves, pushing it back and fully controlling the dynamics of the organ.

3.0.1 Incorporating Dead Cells

To simulate a region of dead cells, the values of u and v are set to the equilibrium values around that specific area. This represents tissue that cannot get excited, and will be unable to propagate electrical signals. This disrupts normal wave propagation, forcing the electrical waves to bend around the inactive region. The sharpest curvatures in the wavefront, where the wave must make the most dramatic directional changes, become focal points for spiral wave formation due to the interaction with the unaltered recovery variable v .

Altering the Initial Gaussian Perturbation:

A Gaussian perturbation can introduce natural curvature and inhomogeneity, increasing the likelihood to induce a breakup when interacting with the non-excitatory region.

To create a vertically stretched perturbation more representative of the normal heartbeat propagation from the sinoatrial node, we can decrease the standard deviation along the x -axis while maintaining a larger spread along the y -axis. Referring back to (11), this is represented as a much smaller σ_X in comparison to σ_Y , to ensure the perturbation is elongated vertically. $\sigma_X = 0.01$, and $\sigma_Y = 1.7$ will be chosen. Essentially, while previously we had small section of broken symmetry at a designated cross section, this will instead create an entire moving wave of spatial inhomogeneity, an improved representation of a simplified heartbeat wave.

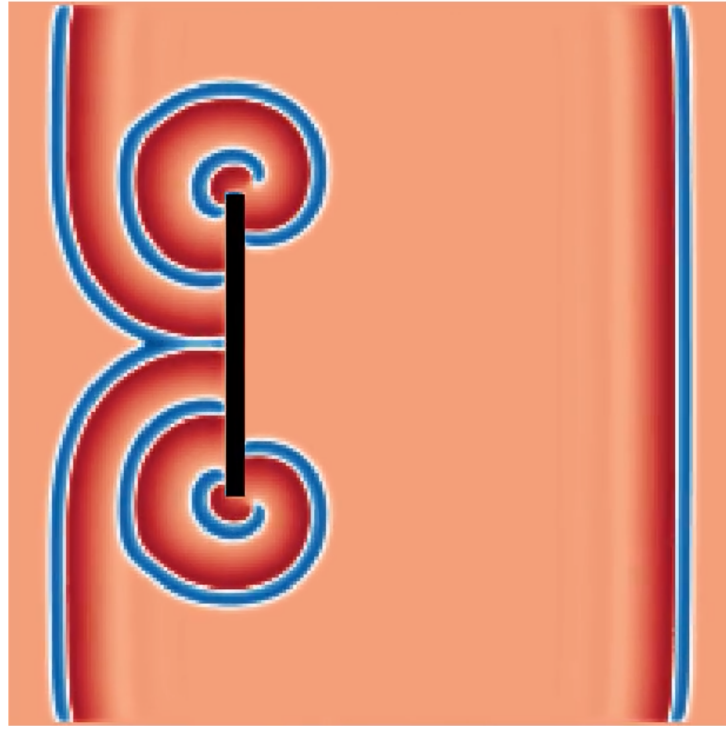
```
1 #setting grid to equilibrium:  
2 u = np.ones((points, points)) * ustard  
3 v = np.ones((points, points)) * vstar  
4 #the vertically stretched gaussian perturbation  
5 X, Y = np.meshgrid(np.linspace(-1, 1, points), np.linspace(-1, 1, points))  
6 stim[15:23] = 0.5 * np.exp(-((X/0.01)**2 + (Y/1.7)**2))
```

Control over the time of this perturbation can also be incorporated with a new computational stimulation method. Putting the perturbation directly inside the du equation grants jurisdiction over when this perturbation is to be applied during the simulation. This method will be utilized further in this project, when the normal heartbeat wave (60bpm) we saw in the introduction will be mathematically represented with periodic gaussian perturbations every second.

```
1 stim = np.zeros((loops, points, points))  
2 du = ((u - (1/3)*u**3 - v + stim[t, :, :]) / epsilon) + L(u)  
3 dv = epsilon * (u + beta - (gamma * v)).
```

The dead cell region remains fixed at equilibrium throughout the entire simulation, preventing excitation and wave propagation.

The Dead Cell Model



To see the full animation visually: [Click Here](#). Additionally, we can plot a static still of the animation at halfway through the simulation time in 3D to convey the dynamics of the system.

The 3D Plot of the Dead Cell Model:

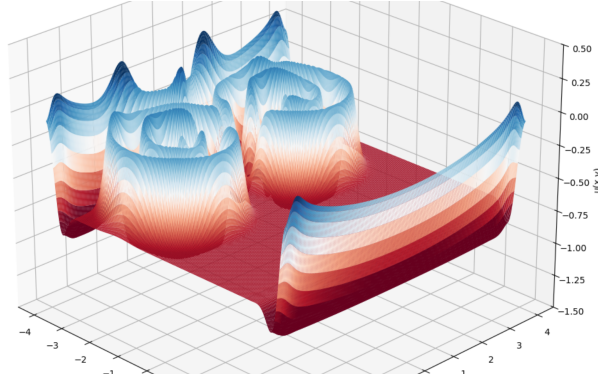
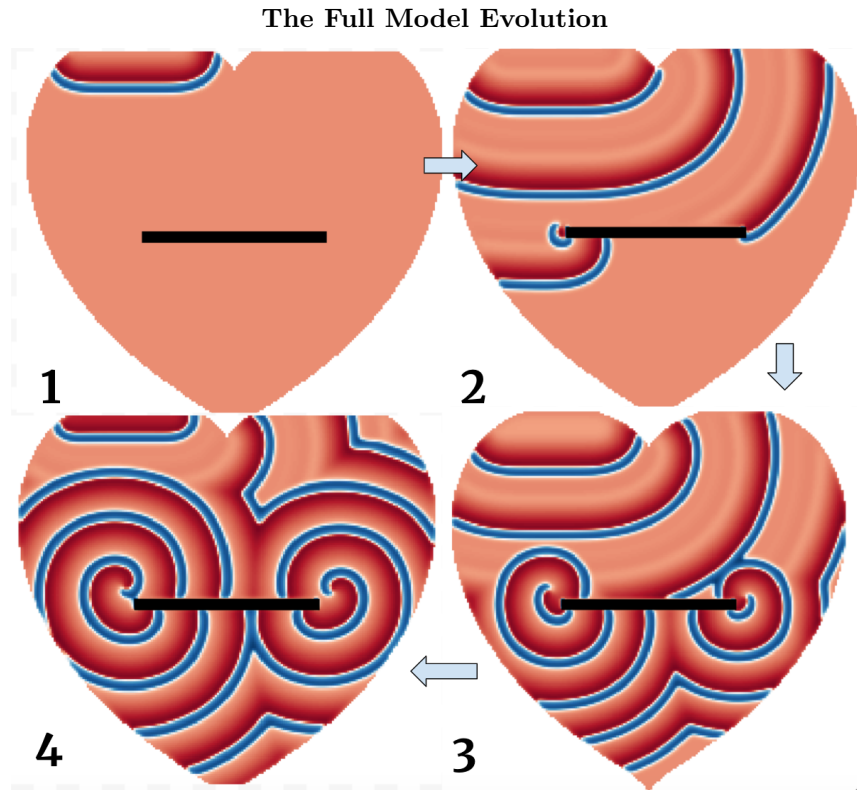


Figure 9: 3D visualization of the FitzHugh-Nagumo dynamics revealing the refractory 'dead cell' region visibly at equilibrium points as well as the recovery variable's effect following the initial excitation wave. Note that the color plotting is the same as the prior 2D model.

Creating the 2D Heart Mask Function: A 2D heart-shaped mask will be applied to the grid for visual purposes, as well as to better represent realistic excitable media, as biological systems rarely conform to simple rectangular domains. Function code: [heartmaskfunction.txt](#). We can utilize this new domain by integrating our existing code into this new border, changing the gaussian perturbation to a horizontal one, shifting its formation to the top left, with one of the two waves propagating downwards through the model. This is a simplified replica of the sinoatrial node emitting heartbeat waves down

through the chambers of the heart.



- **Panel 1:** A normal wave begins to propagate from the sinoatrial node uniformly across the heart, encountering no obstacles or disruptions.
- **Panel 2:** The wavefront reaches the region of dead cells (black rectangle), and the initial disturbance upon contact forces the wave to curve around the unexcitable region, forming the initial spiral structure.
- **Panel 3:** An additional spiral forms later on the right side of the dead cell region. Initial spiral continues to grow.
- **Panel 4:** The spiral waves become fully established and dominate the dynamics of the heart model. They start to push back the regular healthy heartbeat.

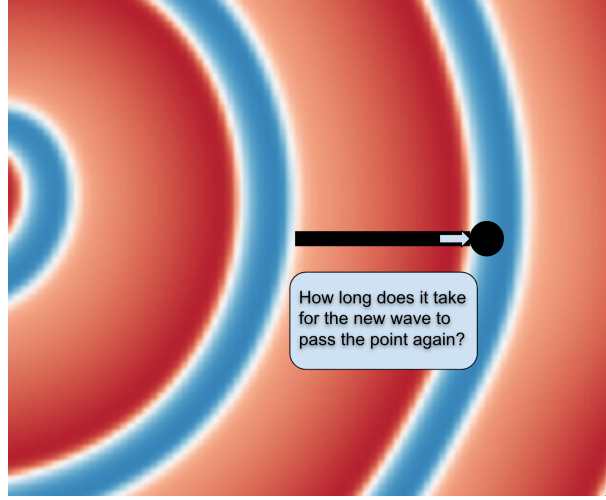
To see the full animation visually: [Click Here..](#)

While it's visible how these spirals outpace the initial heartbeat wave to establish dominance in the model, to understand mathematically how these dynamics emerge and predict their behavior, we need quantitative analysis of their temporal characteristics. We can do this with *period analysis*.

3.1 Analyzing the Period of the 2D Spiral Waves

The period in the context of the spiral wave refers to the time it takes for the wave at a specific point to complete one full oscillation and return to the same phase or value (e.g., hitting a local maximum in u again).

For a spiral wave, this corresponds to the time it takes for the same part of the spiral wave to pass over that point in the grid again. Since the period is the duration between successive peaks, this will be the subject of the model below.



Returning to the default 2D spiral model, the designated point chosen here will be the midpoint, where `mid_idx` is $\frac{\text{points}}{2}$.

3.1.1 Calculating the Average Period

To determine the average period of oscillations:

Identifying Peaks: Local maxima (peaks) throughout the many iterations of the code are identified using the condition:

$$u_t[i - 1] < u_t[i] > u_t[i + 1].$$

The corresponding times of these peaks are stored in an array

```

1 max_times = [
2     times[i]
3     for i in range(1, len(u_t) - 1)
4     if u_t[i - 1] < u_t[i] > u_t[i + 1]]
```

Calculating Periods: The period between consecutive peaks is calculated as:

$$\text{periods}[i] = \text{max_times}[i + 1] - \text{max_times}[i],$$

for all $i = 1, 2, \dots, n - 1$, where n is the number of identified peaks.

```

1 periods = [max_times[i + 1] - max_times[i]
2 for i in range(len(max_times) - 1)]
```

Average Period: The average period is computed as:

$$\text{Average Period} = \frac{\sum_{i=1}^{n-1} \text{periods}[i]}{n - 1}.$$

This value represents the typical time interval between successive oscillations at the midpoint.

```

1 avg_period = sum(periods) / len(periods)
```

Additionally, due to the period undergoing abnormal fluctuations from the initial perturbation in the first few milliseconds of the animation, the average will start after $t = 10$.

Result: After running the code, the printed out Average Period is:

```
1 Average period (after t=10): 11.33 units
```

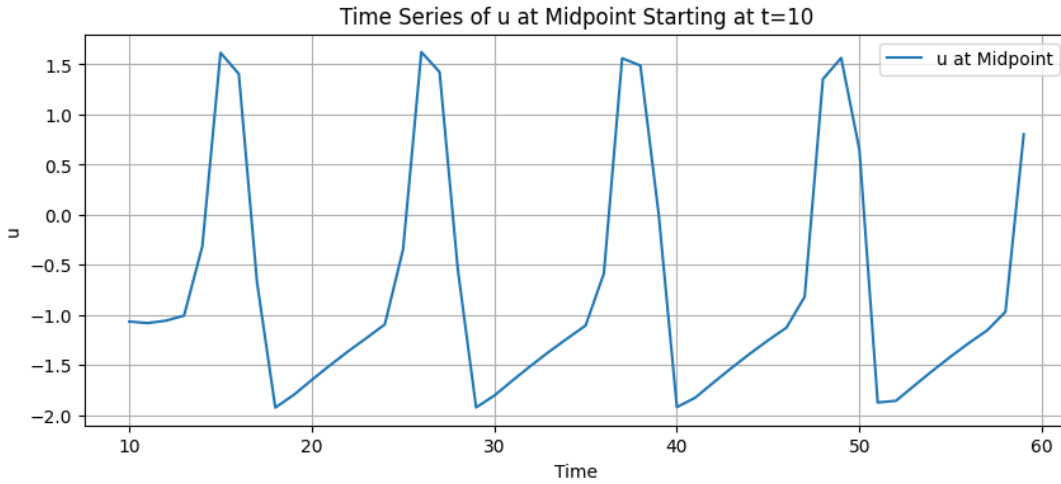
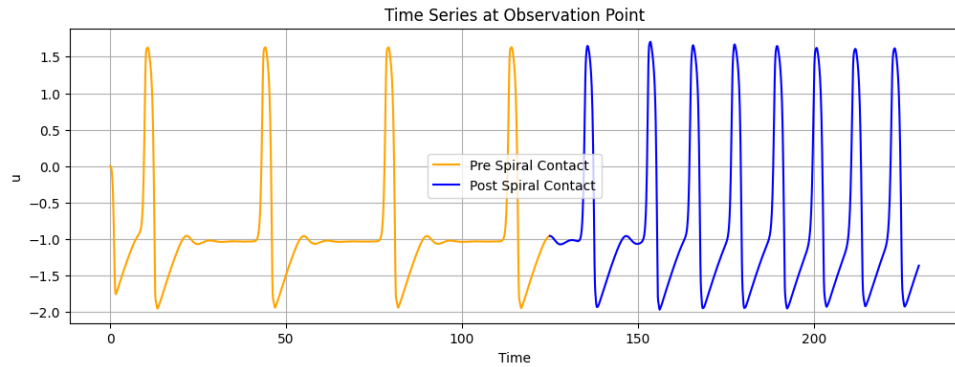


Figure 10: Period graph denoting the peaks of spiral wave contact throughout a designated time period in the simulation. Note that this model uses different time units to future sections, but the mathematical methodologies remain the same.

3.1.2 Measuring the Period of the Dead Cell model:

We recall previously how the dead cell simulation begins with regular heartbeat waves propagating down the domain, but upon impact with the dead cell region, the formed spiral soon dominates the dynamics of the heart, pushing back against the original waves. This alters the period observed at a given point as the spiral's faster rotation shifts the observed oscillations to a new smaller periodicity. The point chosen to measure the period here is (16, 46), in the top left border of the heart.



Initially, regular heartbeat waves are replaced by a more complex pattern as the spiral gains control of the system. On average, the period (distance between peaks) is significantly decreased, meaning the designated point gets 'hit' by more waves, as the spiral oscillates faster.

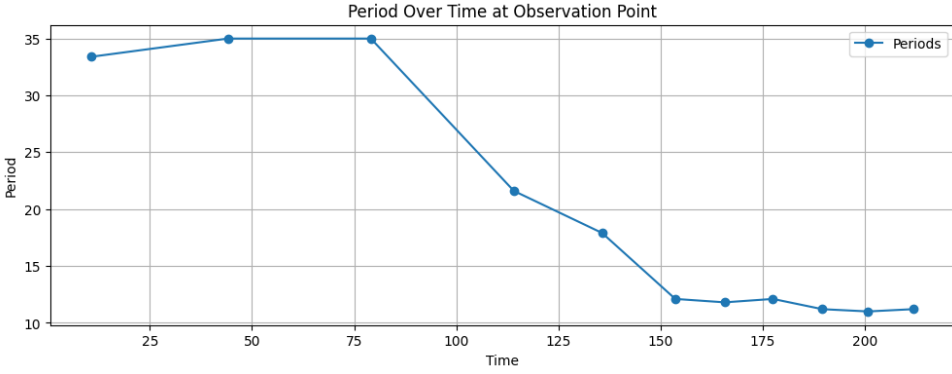


Figure 11: The period at the observation point decreasing due to the spirals faster rotation controlling the system.

Now could this mathematical framework of quantitative wave analysis be utilized to locate the source of the spiral?

3.2 Electrode Probes: Locating the Spiral Source with Triangulation

After understanding how spiral waves affect the period of oscillations at individual points, we can use this knowledge to locate the source of these waves. By placing three measurement nodes, or *probes* at different locations and analyzing when the period changes occur at each node, we can triangulate the spiral's origin. While computationally it would be simpler to scan the entire domain for regions of high curl (something that will be done in a later chapter) to identify the spiral core, our approach mirrors real-world constraints where only a limited number of measurement points are available in cardiac tissue.

In actual medical settings, physicians do not have the have complete visibility of electrical activity throughout the heart. They rely on limited electrode placements, and this following 3-probe method can show how limited sampling on a 2D grid could still enable targeted intervention.

The Basic Principle: When a spiral wave forms, it spreads outward from its source. The time taken for this wave to reach any point is proportional to the distance between that point and the source. By measuring when the period change occurs at three different locations, we can use these timing differences to determine the source location (with a small uncertainty). The reason for 3 is due to how when each node is hit, it comes to a prediction on where it could be, in a radius of a circle around it. If we only had 2, then their overlapping circles would intersect twice, resulting in two possible locations. Thus, three nodes is the minimum amount for a relatively accurate prediction.

For each node, we calculate a distance r using:

$$r = w\Delta t$$

where c is the wave propagation speed and Δt is the time when the period change is detected, the travel time of the wave to reach a designated probe.

The wave propagation speed c can be derived using extensive perturbation analysis by first transforming to spatial wave coordinates and applying linear order analysis, transforming the PDE into a simpler ODE that is more solvable. Since we are interested in the speed at which an excitation propagates through the medium, we seek **traveling wave solutions**, where the system maintains its shape while moving.

For traveling wave solutions $u(x, t) = U(x - ct)$ and $v(x, t) = V(x - ct)$, defining the traveling $z = x - ct$,

we obtain:

$$\frac{\partial u}{\partial t} = -c \frac{dU}{dz}, \quad \frac{\partial v}{\partial t} = -c \frac{dV}{dz}, \quad \nabla^2 u = \frac{d^2 U}{dz^2}.$$

Substituting into the original system:

$$\frac{\partial u}{\partial t} = \frac{1}{\varepsilon} \left(u - \frac{1}{3} u^3 - v \right) + \nabla^2 u, \quad \frac{\partial v}{\partial t} = \varepsilon(u + \beta - \gamma v) \quad (13)$$

Will give the ODE system:

$$-c \frac{dU}{dz} = \frac{1}{\varepsilon} \left(U - \frac{U^3}{3} - V \right) + \frac{d^2 U}{dz^2}, \quad -c \frac{dV}{dz} = \varepsilon(U + \beta - \gamma V). \quad (14)$$

This result is well known in the theory of excitable media and reaction-diffusion where that given ($\epsilon < 1$), it can be shown that the wave speed can be approximated as: $c \approx \sqrt{\frac{D}{\epsilon}}$ where D is the diffusion coefficient [29]. This is a common method in biological models. For the chosen values of $\epsilon = 0.3$ and $D = 1$, this yields $c \approx 1.83$. This computed wave speed, combined with the measured average period of $T \approx 11.33$, shows the relationship $\frac{cT}{2\pi} \approx 3.3$, is a good representation of how the wave propagation speed is related to the period, the spiral's rotational frequency [30].

Next, placing the probes, this creates three circles, each centered at a probe location (x_i, y_i) with radius r_i . The spiral source must lie at the intersection of these circles, giving us the equations:

$$\begin{aligned} (x - x_1)^2 + (y - y_1)^2 &= r_1^2 \\ (x - x_2)^2 + (y - y_2)^2 &= r_2^2 \\ (x - x_3)^2 + (y - y_3)^2 &= r_3^2 \end{aligned}$$

Implementation: First, we detect when each probe experiences a significant period change:

```

1 def analyze_probe_data(data, dt):
2     #with the periods variable we already made:
3     changes = np.abs(np.diff(periods))
4     threshold = np.mean(changes) + 0.5 * np.std(changes)
5     significant_changes = np.where(changes > threshold)[0]
6     if len(significant_changes) == 0:
7         return None
8     transition_time = peaks[significant_changes[0]] * dt
9     wave_speed = 1.83
10    return wave_speed * transition_time

```

Then, we find the point that best satisfies all three circle constraints:

```

1 # Calculate distances from each point to centers
2 d1 = np.sqrt(((points_grid - p1)**2).sum(axis=1)) - r1
3 d2 = np.sqrt(((points_grid - p2)**2).sum(axis=1)) - r2
4 d3 = np.sqrt(((points_grid - p3)**2).sum(axis=1)) - r3
5
6 #Finding the point minimizing total error
7 error = d1**2 + d2**2 + d3**2
8 best_idx = np.argmin(error)
9 uncertainty = np.sqrt(error[best_idx])

```

The uncertainty value tells us how well our prediction fits the data. A lower uncertainty indicates more confident localization of the spiral source.

In practice, probe placement affects accuracy. Ideally, probes should:

- Be placed in different quadrants around the expected spiral region
- Avoid being too close to the heart boundaries
- Form a triangle that surrounds the potential spiral location

But by using this method, we can locate the spiral source with an accuracy typically within 0-7 grid points, depending on probe placement and timing precision. The uncertainty value is due to the spiral tip actually moving slightly over the time period the probes collect prediction data.

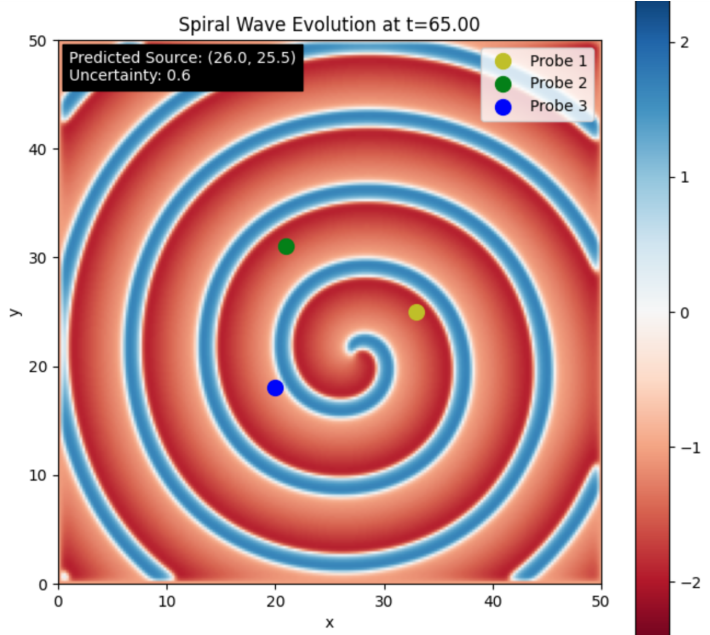


Figure 12: 3 Probes providing a prediction of the source of the default 2D spiral wave.

We can also integrate this method for spiral source detection into the dead cell model. From looking at the animation, it is clear to us where the spiral will form, due to the deterministic nature of this model forming it at the edges of the dead cell regions. But say we had no knowledge of its location, a challenge scientists face in real clinical scenarios, this theoretical method would allow us to find an estimated location of the spiral source, consequently providing an idea of where the dead cell wave break causer lies.

Probe Framework Integrated into the Dead Cell Model

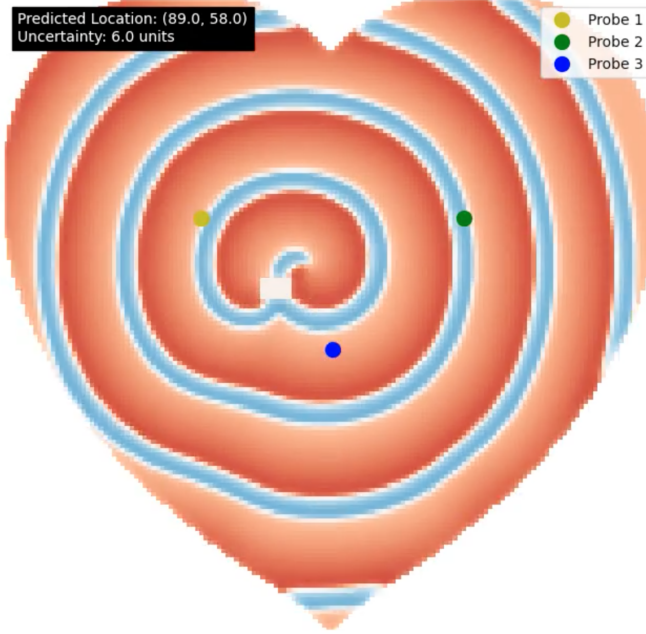


Figure 13: 3 Probes providing a prediction of the location of the dead cells. The uncertainty is slightly higher due to the dead cell interacting with the spiral period. With a smaller designated dead cell region (indicated in white), only one spiral forms.

3.2.1 Applying Targeted Defibrillation with Probe Prediction

Once the probes have provided us with a predicted location (x_p, y_p) of the spiral source, we can apply a localized shock in an attempt to terminate the spiral wave. Before we applied a global shock across the entire domain, but that would require significantly more energy and could potentially damage healthy tissue. With our predicted location, however, we are now able to implement a targeted solution.

Shock Region: Defining a square shock region centered at the predicted location, with side length $l_s = \frac{\text{points}}{4}$. The shock region $S(x, y)$ is defined as:

$$S(x, y) = \begin{cases} A_s & \text{if } |x - x_p| \leq \frac{l_s}{2} \text{ and } |y - y_p| \leq \frac{l_s}{2} \\ 0 & \text{otherwise} \end{cases}$$

with $A_s = 1.0$ as the shock amplitude as before. The shock is applied for a duration $\tau_s = 100$ time steps, starting at time t_s after the prediction is made:

$$u(x, y, t) = u(x, y, t) + S(x, y) \cdot H(t - t_s) \cdot H(t_s + \tau_s - t)$$

where $H(t)$ is the Heaviside step function and $u(x, y, t)$ is the excitation variable.

If the probes location prediction is correct, and the shock region successfully encompasses the spiral core, it will terminate the spiral wave as shown below.

This looks as follows:

The Evolution of the Dead Cell Probe Model w/ a Targeted Defibrillation

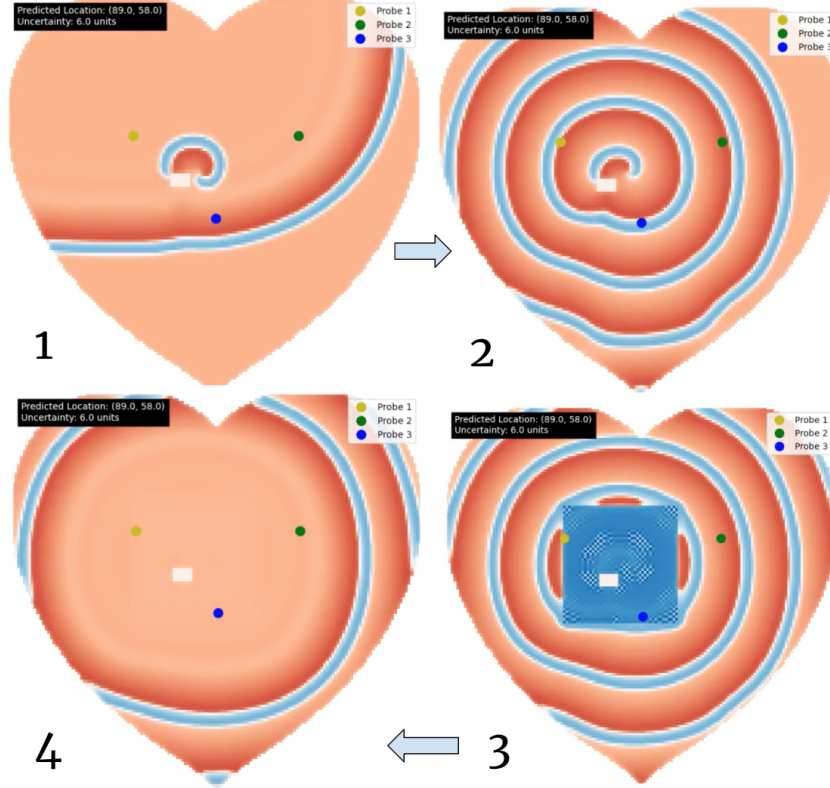


Figure 14: Dead Cell Probe Evolution with a Targeted Shock Defibrillation

The full animation of this evolution: [Click Here:](#)

- **Panel 1:** As before normal wave propagates uniformly across the heart, forming a spiral upon contact with the dead cell region. (the probes are coded to ignore the initial healthy heartbeat wave)
- **Panel 2:** After the spiral is fully established and grows, the probes make their prediction on the location of the source (consequently next to the dead cells).
- **Panel 3:** Once they make their prediction, after time t_s a shock is applied directly centered on that prediction
- **Panel 4:** The prediction was accurate. The source of the spiral has successfully been terminated, there are no more perturbations, and its remaining formed waves trail off.

This works for other locations of the dead cell and varied positions of the three probes as well, see another animation of this evolution with a varied dead cell location and probes: [Click Here:](#).

However, there is a chance if it does not encompass the entirety of the spiral source, multiple spirals could occur.

A Misprediction

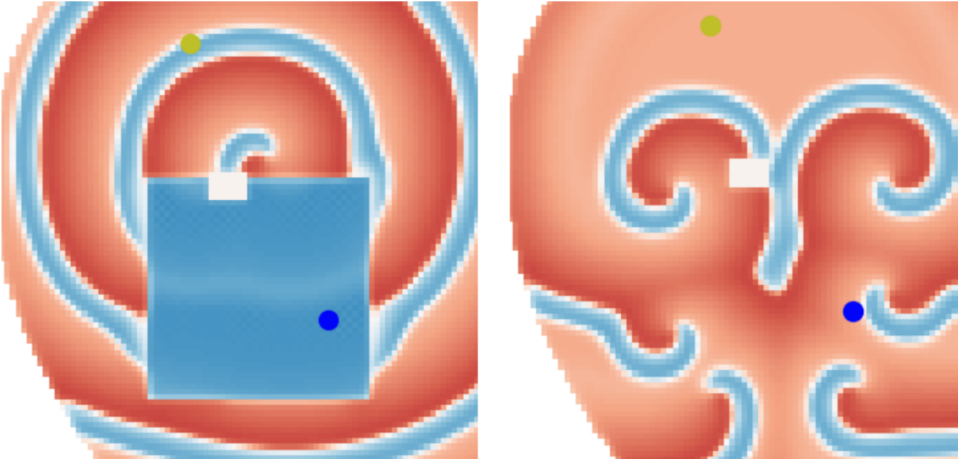


Figure 15: The targeted defibrillation misses due to its high uncertainty value from the electrode probe locations

The uncertainty number is too large in this scenario, due to the third node being in the far bottom right of the heart (not shown in model). The defibrillation shock applied misses the the spiral core, and as a result, this large stimulus instead creates new spirals.

While our analysis focuses on a 2D slice, extending this to 3D would provide a more realistic representation of cardiac modeling. Fully animating this in 3D would not be computationally feasible, but the methodology remains the same, except with additional probes required to provide the necessary depth of information.

A Theoretical Extension to 3D Spiral Source Localization:

To extend our 2D triangulation method to three dimensions, we would instead require four probes to uniquely determine the spiral source location. Each probe at position (x_i, y_i, z_i) detects the wave at time t_i , defining a sphere:

$$(x - x_i)^2 + (y - y_i)^2 + (z - z_i)^2 = r_i^2, \quad (15)$$

where $r_i = c\Delta t_i$ is the estimated distance, with our wave speed c and time difference Δt_i .

The reasoning for needing four probes is as follows:

- Two spheres intersect in a circle (infinite solutions)
- Three spheres intersect at two points (ambiguous solution)
- Four spheres determine a unique point (when non-degenerate)

With four nonlinear equations for the unknown position (x, y, z) , it's theoretically sufficient, however, the accuracy still depends on probe placement as poorly distributed probes can lead to systems with large numerical errors, as observed in the 2D simulations.

Bridging Theory to Existing Clinical Implementation:

In practice, while the invasive nature of inserting probes directly into 3D cardiac tissue may be clinically challenging, the overall methodology remains the same. Modern cardiac mapping techniques consist of methods such as:

- **High-density electrode arrays:** 50+ electrodes on catheter surfaces or patches
- **Phase mapping:** Reconstructing rotor core locations from surface measurements
- **Non-invasive mapping:** Simple, body surface electricity mapping using 200+ external electrodes.

These use the same mathematical principle established here, utilizing multiple artificially added measurements to find arrhythmia sources.

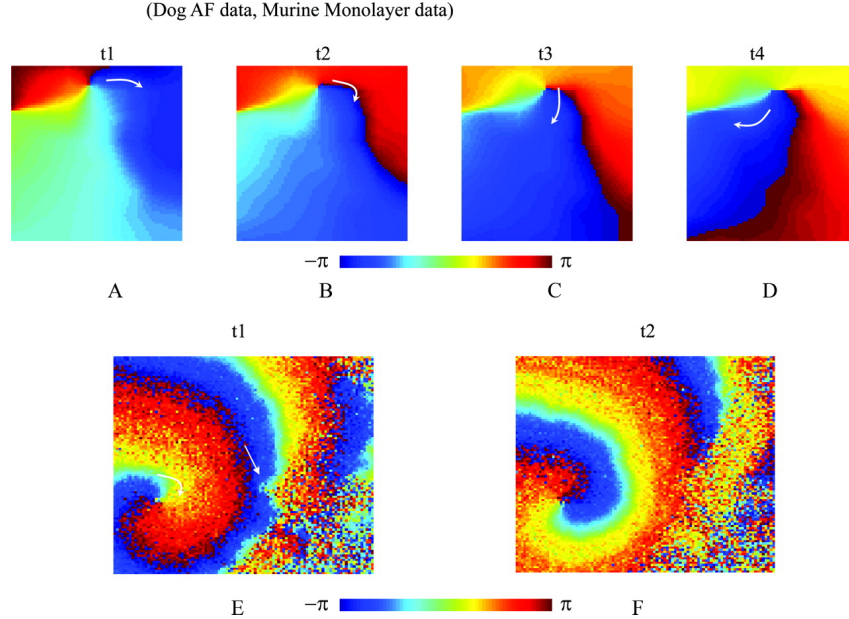


Figure 16: Phase maps from the American Heart Association [31]. Top row shows 4 instances of phase maps constructed through electrode arrays. Bottom panel (E and F) shows 2 phase maps with clear rotor spiral rotations.

This mechanistic approach to spiral wave formation has been validated in clinical settings. Studies using phase mapping techniques have successfully identified spiral waves (clinically referred to as rotors) in human hearts during arrhythmias, confirming their existence beyond theoretical models. As shown above by the AHA and by Gray et al. [33], phase maps constructed through electrode arrays can visualize clear rotor formations, allowing clinicians to pinpoint wave breaks (see white arrow in Figure E).

However, these clinical observations reveal something very important. Unlike the stable spirals in our deterministic models, mapped spirals frequently exhibit significant meandering and variability [34]. Rotors observed during mapping often arise with a little to no warning, have short lifespans, sometimes lasting only a few rotations before terminating or moving to new locations. This observed instability suggests our deterministic framework captures only a small sliver of the complex reality of this vital organ.

A Methodological Pivot: From Deterministic to Stochastic Modeling

Thus far, we have demonstrated that spiral waves can be generated in excitable media using the Fitzhugh-Nagumo model through two deterministic mechanisms:

- **The Gaussian Perturbation:** A precisely defined mathematical construct applied at specific locations and predetermined times, offering complete control over spiral initiation.
- **Dead Cells:** Fixed non-excitatory regions that will create predictable wave-breaks, forcing normal waves to interact, bend, and form spirals deterministically.

These approaches have allowed us to develop a connection between our framework and clinical reality, notably the targeted interventions via probe guided defibrillation. However, as the aforementioned research and clinical phase mapping evidence demonstrates, there exists a fundamental gap between our idealized models and biological reality. Cardiac tissue operates with innate variability in its anatomical processes, including fluctuations in concentrations of electrolytes, spatiotemporal heterogeneity in damaged tissue properties, and metabolic processes that vary across cells and regions. These factors contribute to the unpredictable behaviors observed in clinical settings.

To address this issue and bridge the gap between mathematical convenience and physiological reality, we shall now enhance our existing framework with **stochasticity**, incorporating variability as an essential feature in our models.

4 Representing Cardiac Diseases in the Heart with Electrolyte Stochasticity

Building upon our methodological shift toward biological realism, we shall now examine how the variability in cardiac dynamics can be modeled.

At the molecular level especially, ion channel gating is fundamentally probabilistic. The opening and closing of the voltage gated channels in cardiac cells follows statistical rather than deterministic rules. These microscopic fluctuations create inherent 'noise' in membrane potential that is clinically shown to become much more pronounced with age and disease [1], [35-37]. Furthermore, calcium dynamics in the cells exhibit a degree of statistical variability, with calcium "sparks" (discrete, localized release events) occurring randomly causing slight variability in action potential duration.

While nature is never perfect, some degree of this aforementioned variability is normal and even necessary for healthy function. But excessive fluctuations under a weakened organ are often the cause for arrhythmias. As cited, among all components of cardiac physiology, electrolyte dynamics best represent the perfect combination of deterministic processes and inherent randomness, and will be the focus of our bridge from the mathematical Fitzhugh-Nagumo equations to real-world clinical results.

Cardiac electrophysiology depends critically on the precise balance of ions across cell membranes, regulated rigorously by four key electrolytes: Potassium, Sodium, Calcium, and Magnesium. These electrolytes control the cardiac cycle, represent a primary source of statistical variability, and their imbalances can lead to spiral waves characteristic of cardiac diseases. Due to their microscopic, unpredictability, stochasticity is the best choice to represent their imbalances.

The more complex Hodgkin-Huxley equations, referenced in the first chapter directly accommodate ion channel dynamics for specific electrolytes. While our Fitzhugh-Nagumo model simplifies these detailed ionic mechanisms into our variables u and v , the underlying principles remain connected to electrolyte balances. Therefore, their introduction into this report was inevitable, and a breakdown on the basics of their function is required.

4.1 Electrolytes and Cardiac Wave Propagation: The Basics

Electrolytes (Na^+ , K^+ , Cl^-) enable heart electrical activity through two ways. First, **Voltage Creation**, where different concentrations of ions inside vs. outside cells create electrical voltage across cell membranes. Second, **Electrical Waves**: When triggered, ion channels open in sequence:

- Sodium rushes in → cell becomes positive → activates neighboring cells
- Potassium flows out → cell resets → prepares for next wave

Additionally, an *Action Potential* refers to this rapid rise and fall in electrical membrane potential that occurs when a nerve or muscle cell is stimulated. In cardiac cells, it's essentially the threshold for an electrical signal that allows the heart to contract in a healthy manner.

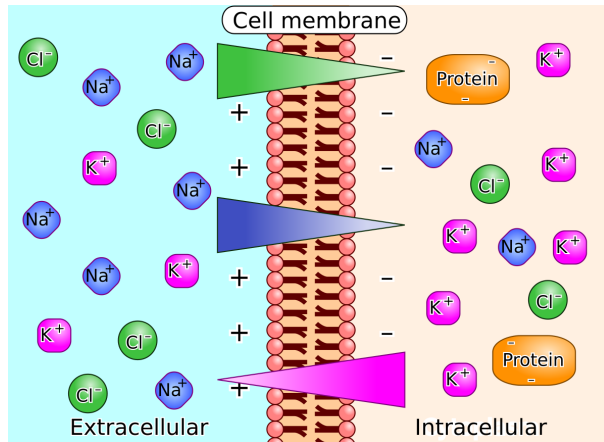


Figure 17: Extracellular: High Na^+ and Cl^- , low K^+ . Intracellular: High K^+ , low Na^+ . Cell membrane: Acts as a barrier, maintaining charge differences. Ion gradients: Arrows indicate movement of ions. [18]

4.2 Modeling Electrolyte Imbalances as a Source of Cardiac Stochasticity

Imbalances in these aforementioned electrolytes are typically as follows:

- **Potassium imbalances** (normal: 3.5-5.0 mEq/L): Both hypokalemia (potassium levels slightly lower) and hyperkalemia (potassium levels slightly higher) affect action potential duration. Synonymous with the threshold for excitation, this will be manifested in our model with β .
- **Calcium disturbances** (normal: 8.5-10.5 mg/dL): Affect contractility, creating temporal heterogeneity in action potentials. As this affects the overall recovery period, it will be represented in this framework as ϵ .
- **Sodium abnormalities** (normal: 135-145 mEq/L): Influences conduction speed across cardiac tissue via depolarization, also tied to ϵ .
- **Magnesium fluctuations** (normal: 1.5-2.5 mg/dL): Moderates overall cellular excitability.

These imbalances contribute to spiral wave formation through three key mechanisms:

(1) **Spatial Heterogeneity**: Creating regions with different *refractory periods*, the time after a cell fires when it cannot be re-excited. For example, a wave propagating downward in a region with different refractory periods can then re-enter excitable tissue, forming a circulating spiral wave.

Clinical measurements have revealed that regions with variable potassium concentrations create patches of cardiac tissue with significantly different refractory periods. The Rotterdam Study demonstrated this directly contributes to arrhythmia vulnerability, with hypokalemic patients showing a 63% increased risk of developing atrial fibrillation (Van Der Ende et al., 2013) [25], [36].

(2) **Temporal Instability**: Altering the *rate* of recovery times in the refractory periods, often related to varied K^+ , Cl^- .

Research by Koretsune et al.(2015) demonstrated that calcium handling abnormalities create temporal instability in cardiac action potentials, though their influence on arrhythmia susceptibility appears less pronounced than potassium channel disruptions [34], [37].

(3) **Conduction Abnormalities (low Na^+)**: Similar to the dead cell model, electrolyte imbalances can too, create barriers that slow the heartbeat wave down or make it unidirectional (i.e., a wave can pass in one direction but not the other), potentially forming a wavebreak, essential for spiral formation. Zhang

et al. showed computational models incorporating potassium channel mutations created unidirectional blocks similar to structural obstacles, forming the essential substrate for reentrant circuits [38].

The next 3 sections will explore how stochastic processes integrated into the FitzHugh-Nagumo framework can represent physiological variability in cardiac tissue with different methods and parameters. This will represent a fundamental shift in this work, deliberately relinquishing our control over deterministic timing and control of spiral formation, but in turn, enhancing the level of modeled realism. We shall examine two key types of noise that model different aspects of electrolyte-driven variability:

- **White Noise:** An introduction to noise. Represents completely independent fluctuations in time and space. In biological representation, it has its drawbacks, but is most analogous to instantaneous variations in ion channel gating.
- **Coloured Noise:** The main focus of the remainder of this report. Incorporating temporal and spatial correlations through the Ornstein-Uhlenbeck process, mirroring how most clinically significant electrolyte abnormalities develop and persist with temporal correlation, and how they can effect the overall system.

Additionally, we can also connect these statistically driven cardiac models with a realistic connection of age-related variability. Age-related changes in cardiac tissue present a significant challenge in understanding arrhythmia development. As documented by Hayano & Yamada [2], aging hearts show increased oxidative stress and higher rates of cardiomyocyte death, leading to more variability in electrolyte imbalances and activity.

4.3 The Additive White Noise Model

Can Stochastic Noise solely induce Spiral Waves in this System?

To begin our exploration of stochasticity, we first investigate whether simple random fluctuations can generate spiral waves without external stimuli. Real cardiac electrolyte dynamics involve complex ionic mechanisms with temporal dependencies, but as an initial approximation, we can model these using a Wiener process $W(t)$. This process represents independent random fluctuations where each grid point (representing a cell, or small region of cardiac tissue) receives uncorrelated noise at each time step, implemented as $\sigma\sqrt{\Delta t} \cdot Z$, where Z is a standard normal random variable. While this white noise approach lacks the memory effects observed in actual ion channel gating, it serves as an instructive starting point to isolate the effects of pure randomness on spiral formation.

Mathematical Framework: The Wiener process $W(t)$ has the following properties:

- Mean: $\mathbb{E}[W(t)] = 0$ and Variance: $\text{Var}[W(t)] = t$
- Independent increments: $W(t + \Delta t) - W(t)$ follows $\mathcal{N}(0, \Delta t)$

For a stochastic differential equation of the form:

$$dx = f(x, t)dt + \sigma(x, t)dW(t) \quad (16)$$

We use the Euler-Maruyama method:

$$x_{t+\Delta t} = x_t + f(x_t, t)\Delta t + \sigma(x_t, t)\sqrt{\Delta t} \cdot Z \quad (17)$$

Application to FHN Model: Applying this framework to our FHN model, we add noise to the variable u :

$$u_{t+\Delta t} = u_t + du \cdot \Delta t + \sigma\sqrt{\Delta t} \cdot Z \quad (18)$$

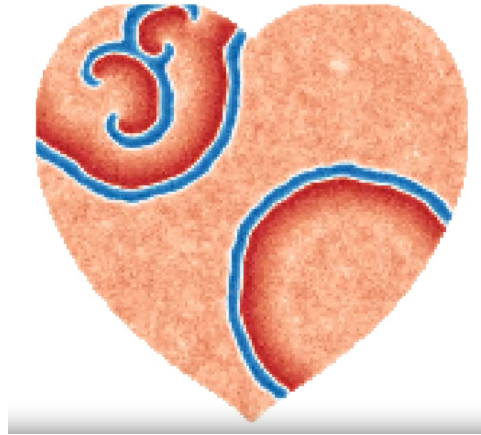
where σ controls the noise amplitude and $\sqrt{\Delta t}$ properly scales the noise term for each time step. All points in the grid will also be set to equilibrium (u^*, v^*). The Laplacian will also be excluded from potential noise generation, because when noise interacts with the Laplacian at the boundaries (where there is a sharp gradient or change in the field), the properties of the second derivative essentially amplify these small levels of noise, causing a larger magnitude, controlling the framework. Additionally, since added fluctuations on the recovery of the Fitzhugh-Nagumo do not cause significant changes in the dynamics of the system, this noise will not be applied to the v variable.

```

1 interior = mask & ~border #excluding borders
2 u += (noise * sqrt_dt * np.random.randn(points, points)) * interior

```

The White Noise Model: ($\sigma = 0.23$)



Here is a snapshot and animation of the model at $\sigma = 0.23$. Increasing σ would result in more perturbations. This proves our hypothesis that background noise can generate re-entry spiral patterns without any external stimuli. To watch the full animation: [Click Here](#):

To find a lower bound, we can also look at what happens when we decrease σ further to $\sigma = 0.20$, a noise value that is not strong enough to generate spirals. But we can below see that if we include the noise into the Laplacian borders, that the lower bound of $\sigma = 0.20$ is indeed sufficient to generate spirals in that system. This increased concentration or accumulation of the noise near the boundary is enough to generate its own spirals at a lower σ threshold, even when the noise in the interior is insufficient on its own. Animation: [Click Here](#):

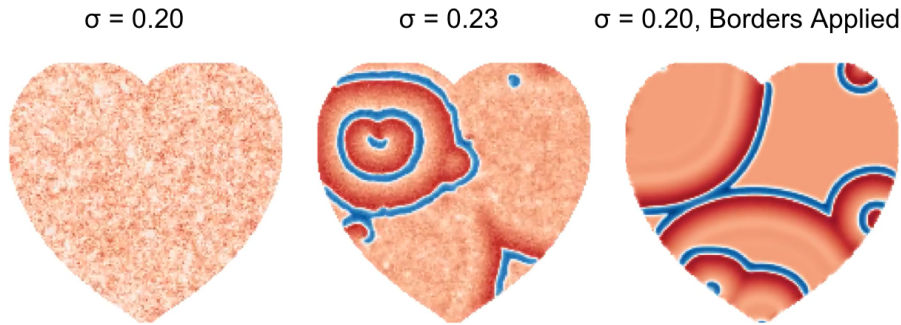


Figure 18: Left: Low white noise with borders excluded. Middle: Average white noise with borders excluded. Right: Low white noise, but borders are not excluded.

Biological Limitations of White Noise: It's important to recognize where white noise diverges from reality. Ion channel dynamics in cardiac tissue demonstrate significant temporal correlations, where the state of a channel at time t influences its behavior at time $t + \Delta t$. For example, potassium channel recovery follows exponential time constants rather than instantaneous random transitions. Similarly, calcium spark propagation exhibits spatial correlation across adjacent regions of the sarcoplasmic reticulum. White noise, with its property of independent increments, cannot capture these memory effects. Therefore, we require a more sophisticated stochastic framework.

An ideal model should incorporate:

1. **Memory effects**, where past states influence future behavior.
2. **Mean-reverting tendencies**, reflecting homeostatic mechanisms.
3. **Controlled variance**, representing different pathological states.

The Ornstein-Uhlenbeck process addresses these requirements, making it substantially more appropriate for modeling the complex dynamics of cardiac electrolytes. We explore this approach in detail below.

4.4 The Coloured Noise Model: The Ornstein-Uhlenbeck Process

The Ornstein-Uhlenbeck (OU) process is a colored noise Stochastic Differential Equation (SDE) that introduces temporal correlations into our model. Unlike white noise where each value is independent, the OU process has "memory", meaning each fluctuation depends on its previous state. This will be the core representation of our newly defined ion channel electrolyte system, where heart cell fluctuations influence future states rather than occurring as isolated, independent events. For example, electrolyte imbalances in the heart will rarely develop as instantaneous fluctuations, but rather with temporal correlation as ions diffuse through the cellular exterior and affect the nearby adjacent cells. Here is a specific numerical example of this: [Example](#). This makes the OU process a preferred method for modeling these chemical disturbances in heart cells, as utilized frequently by researchers, and it will be the default framework for the next chapter as well.

4.4.1 Mathematical Definition

The Ornstein-Uhlenbeck (OU) process is defined by the stochastic differential equation:

$$dX_t = -\theta(X_t - \mu)dt + \sigma dW_t$$

X_t : Noise value at time t

μ : Mean (baseline) value

θ : Speed of reversion to mean

σ : Intensity of randomness

dW_t : Small white noise increment

Updating the noise at each timestep using the OU formula:

$$X_{t+\Delta t} = X_t + \Delta t \cdot (-\theta(X_t - \mu)) + \sigma \sqrt{\Delta t} \cdot Z_t$$

where $Z_t \sim \mathcal{N}(0, 1)$

Parameter effects: θ controls noise frequency (high: rapid fluctuations, low: slow changes); σ controls strength (high: significant perturbations, low: subtle nudges).

Code for the OU function:

```

1 def ou_noise(current, theta, mu, sigma, dt, shape):
2     dW = np.random.randn(*shape) #note that 'shape'=(points,points)
3     next = current+dt*(-theta*(current-mu)) + sigma*np.sqrt(dt)*dW
4     return next

```

As with the white noise, this Stochastic Differential Equation will be added to the u excitatory variable at all points in the grid except the borders, and at every iterative time step. This colored noise will not be applied to the v recovery variable as well. With our mathematical framework established, the Ornstein-Uhlenbeck noise parameters (θ, σ) can be interpreted in terms of real cardiac electro-physiological behavior. By varying these parameters, we can observe behavior similar to many different types of cardiac arrhythmia's. Referencing and applying Cartier's observational analysis for the Ornstein Uhlenbeck process, we can come to a relatively concrete classification of parameter ranges and their real life relevance [38].

Low Stochasticity ($\theta > 0.01, \sigma \leq 0.01$): Representing normal physiological variability in healthy cardiac tissue. This represents normal physiological variability in healthy cardiac tissue with well-regulated electrolyte concentrations.

Moderate Stochasticity ($0.01 \geq \theta, \sigma \leq 0.02$): Modeling increases in cellular variability, perhaps due to age-related system changes, these parameters could represent potential arrhythmia representation. These parameters could model mild electrolyte disturbances seen in conditions such as early stage hypokalemia or hyperkalemia.

High Stochasticity ($\theta \leq 0.01, \sigma \geq 0.02$): Representing pathological states that could lead to deadly arrhythmias. For example, profound hyperkalemia, when the potassium levels, (a key factor in affecting action potential duration) are too high, decreasing the threshold for unwanted electrical activity to occur.

Mathematically, there is a connection between the values of θ and σ , as an increased value of θ , meaning a stronger 'pull' to equilibrium requires a higher σ value to generate stronger fluctuations to compensate for it in terms of generating spirals. We will then create stochastic animations of selected parameters in these ranges, and observe if they can represent cardiac diseases and arrhythmias.

Time Dimensionalization for Period Analysis:

An effort to dimensionalize our iterative simulation parameters with real time is required here to truly convey the harmful effects of the represented cardiac arrhythmia that follow. In our new model, each time unit equates to 60 milliseconds. 100 time units is 6 seconds. The entire simulation length for the following simulations is 160 time units, thus, around 10 seconds of real animation time. However, for the proceeding period analysis of each disease, only 100 time units will be measured, to account for the time required for the initial wave to hit the designated measuring point.

4.4.2 Low Parameter Values: Normal Heart Behavior

Parameters ($\theta = 0.01, \sigma = 0.01$) applied to our original healthy heartbeat waves. As can be seen in the animation, without an external influencing factor (ex. fibrosis) this shows no significant difference in the fundamental nature of the system. This will be used heavily after this chapter, where small insignificant fluctuations in e.g ion channel dynamics have no effect on cardiac disease formation, but can slightly alter the dynamics of the system, incorporating a small level of unpredictability, providing a more realistic representation of the heart.

Animation: [Click Here](#):

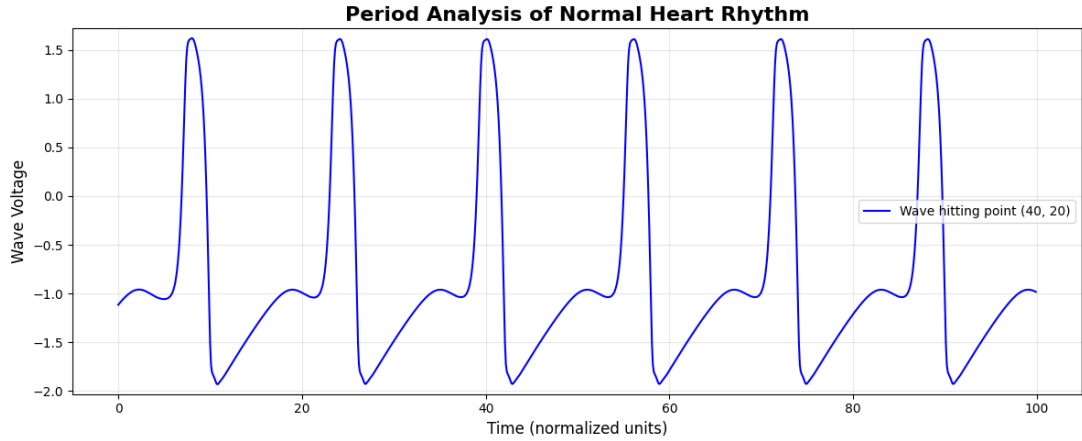


Figure 19: A representation of a biologically realistic normal heartbeat. With no change in the system's dynamics, the period analysis is unaltered, with the heart rate accurately portraying 60 beats per second. Electrolyte concentration is healthy.

4.4.3 Moderate Parameter Values: Tachycardia-Like Behavior

Moderate noise parameters ($\theta \approx 0.018, \sigma \approx 0.016$) as seen below can generate spiral perturbations. As no two animations in stochastic modeling are the same, we can see that in this specific simulation, two merged spirals appear, albeit, similar to our standard 2D spiral we have seen previously.

Clinically, this pattern is often associated with moderate electrolyte abnormalities such as moderate hypokalemia (3.0-3.5 mEq/L), consistent in aging hearts [2]. These imbalances, associated mathematically with the moderate θ and σ values, create enough instability to initiate non chaotic, organized spiral formation. Still, this spiral will outpace the hearts normal rhythm significantly. [Animation](#):

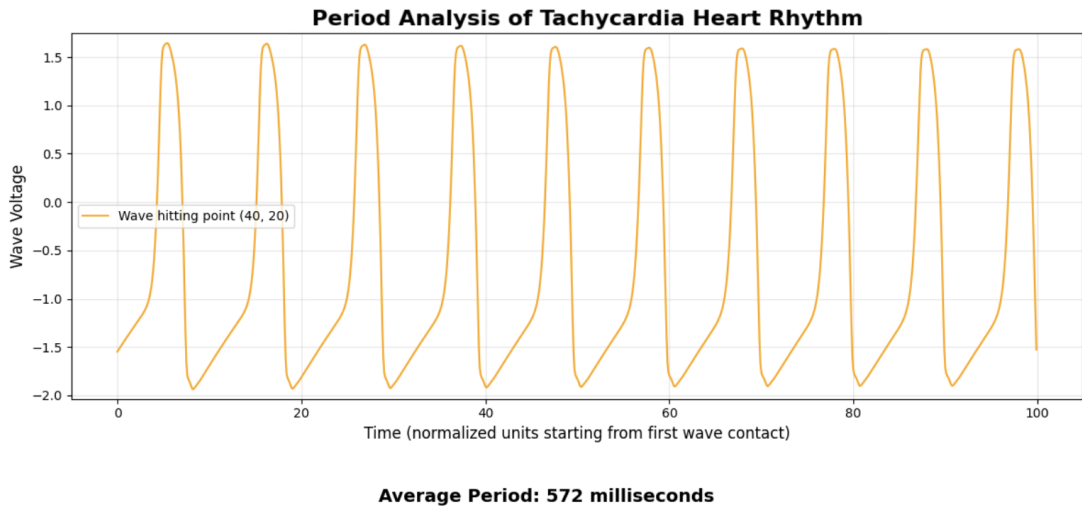


Figure 20: Period analysis of Tachycardia with average noise parameters.

By selecting a random point on the grid, and measuring the average period only when the first wave hits the point, we can see that the average period is significantly lower than our healthy heart's. Connecting artificially dimensionalized time units to clinical data one-to-one can provide its challenges, but Stanford Health Care notes that Tachycardia may occur at rates as low as 110 bpm, equating to a cycle length of about 545 milliseconds [32].

Visualization of Tachycardia, ($\theta = 0.018, \sigma = 0.016$)



Figure 21: A representation of Tachycardia with average noise parameters.

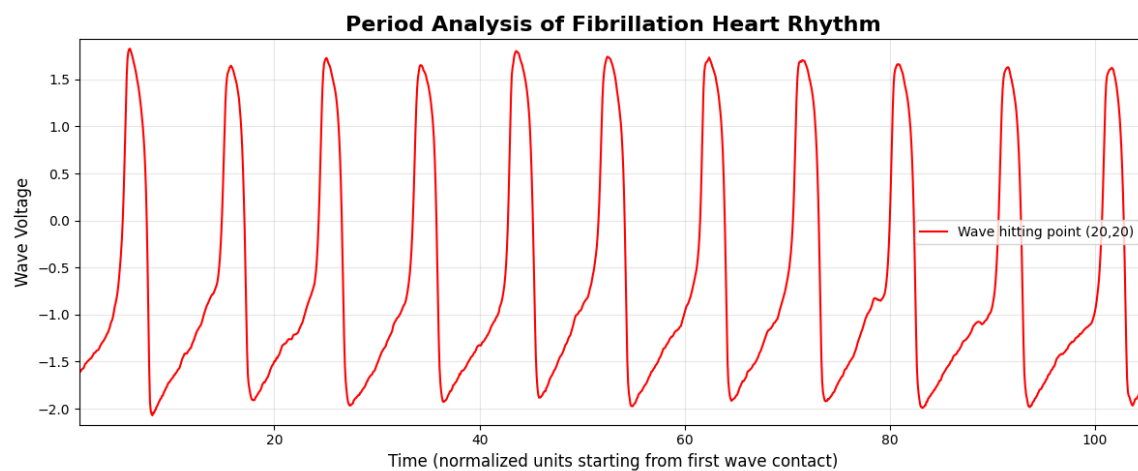
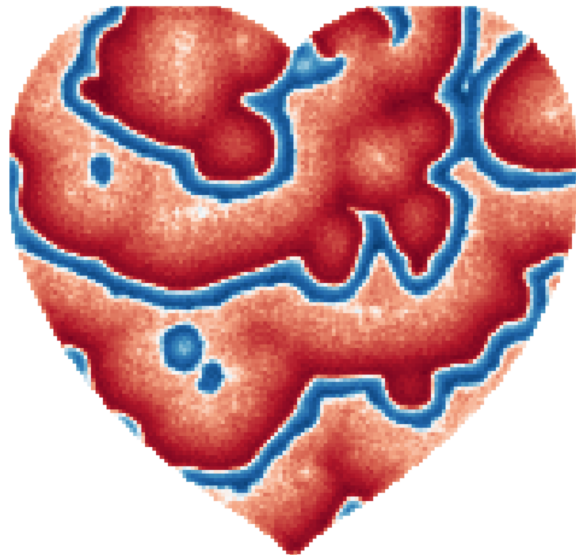
4.4.4 High Parameter Values: Fibrillation-Like Dynamics

As we decrease the speed of reversion to the equilibrium (θ), even further, and increase the strength of the fluctuations (σ) once more, the parameters ($\theta \leq 0.01, \sigma \geq 0.02$), transition the system to more chaotic behavior characteristic of *Ventricular Fibrillation* a very harmful disease:

- Higher θ values reduce the temporal correlation, creating more rapid fluctuations
- Increased σ leads to multiple waveform breakups and spiral wave fragmentation
- The combination results in multiple, unstable rotating waves that continuously interact and break up, very similar to the chaotic electrical activity during fibrillation.

Multi-electrolyte disturbances, common in conditions like severe renal failure or drug toxicity, typically produce this pattern, as severe abnormalities in potassium, calcium, and magnesium levels disrupt the entirety of the cardiac action potential. This essentially alters the resting membrane level, decreasing the threshold for perturbations to occur, thus, creating the chaotic disordered wave fronts seen below.
Animation: [Click Here](#):

Visualization of Fibrillation, ($\theta = 0.01, \sigma = 0.022$)



With an average period of 418 milliseconds, we observe that not only this heart rate faster (140 bpm), but due to the variance in distance between peaks, the heart rate is also **irregular**. Progression from tachycardia to fibrillation is possible, and it often reflects worsening electrolyte homeostasis.

Without immediate treatment, a ventricular fibrillation rhythm is fatal. For each minute you wait for defibrillation, your chance of survival drops by 7-10 percent [20].

An animated comparison between tachycardia and fibrillation: [Click Here](#):

5 Fibrosis: Regional Tissue Variation

What is Fibrosis?

Fibrosis is the excessive formation of connective tissue in an organ, usually as a response to injury, inflammation, or stress. In the heart, cardiac fibrosis is formed typically in result of a heart attack, and replaces the normal heart muscle cells with fibrotic (scar) tissue. This tissue is inherently weaker, and depending on the severity, can disrupt electrical signaling and can increase the risk of arrhythmias.

Fibrotic tissue slows down wave conduction, leading to higher levels of anisotropy in that region. This non-uniformity creates areas where normal waves break down into chaotic reentry patterns, forming spiral waves. This effect is often exacerbated by electrolyte imbalances that develop around fibrotic tissue, as scar formation disrupts normal ion channel distribution and hinders electrolyte diffusion. The increased tissue heterogeneity from fibrosis makes Tachycardia and even Fibrillation more likely, as electrical waves get trapped in reentrant circuits [31].

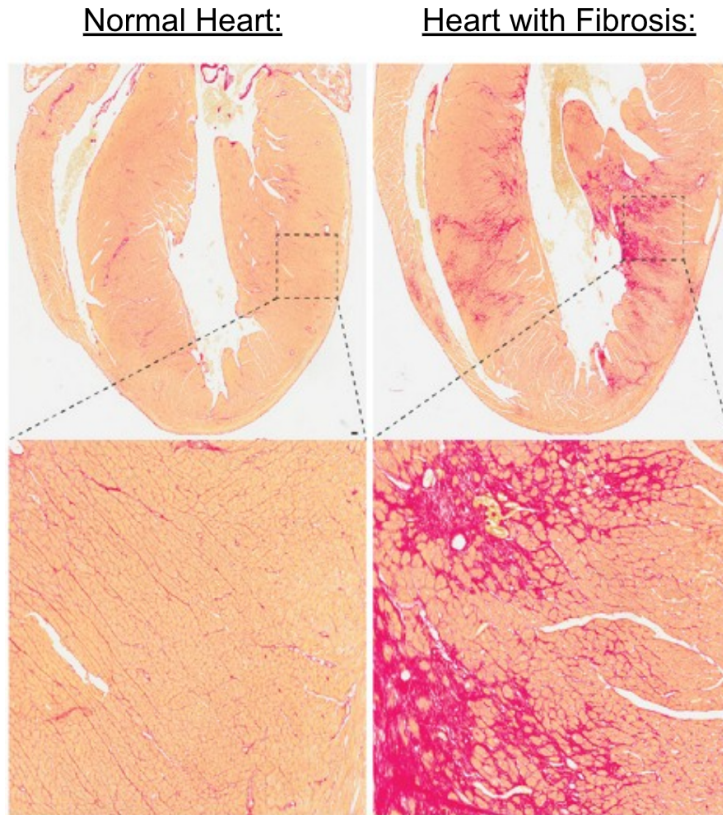


Figure 22: A real life comparison of a normal heart and a heart with fibrosis scarring [19]

Mathematical Implementation

To represent Fibrosis, we will represent this biological heterogeneity by coding a region ($\frac{points}{6} \times \frac{points}{6}$) in the grid with altered FHN parameters below. Low OU coloured noise parameters ($\theta = 0.01, \sigma = 0.01$) will also be applied to the entirety of the grid, providing a more physiologically relevant representation of fibrosis-affected tissue, where small conduction variabilities are common. For the designated damaged region itself, we can represent this with altered FHN parameters: $\epsilon = 0.27$ and $\beta = 0.67$.

- Higher excitability ($\epsilon = 0.2.7$ vs 0.3) - More sensitive to stimulation
- Lower activation threshold ($\beta = 0.67$ vs 0.7) - Easier to trigger

Effect of Decreasing ϵ :

In the FHN equations:

$$\frac{\partial u}{\partial t} = \frac{1}{\varepsilon} \left(u - \frac{1}{3}u^3 - v \right) + \nabla^2 u, \quad \frac{\partial v}{\partial t} = \varepsilon(u + \beta - \gamma v)$$

When ϵ decreases:

- The $\frac{du}{dt}$ term becomes larger as $\frac{1}{\epsilon}$ increases
- The $\frac{dv}{dt}$ term becomes smaller as ϵ decreases

This creates a stronger separation of timescales between the excitatory (u) and recovery (v) variables. The increased ratio between these timescales ($\frac{1}{\epsilon^2}$) makes the system more prone to oscillatory behavior, as recovering back to equilibrium takes longer with respect to time, thus, allowing more time for perturbations to occur.

Biological Connection: A lower ϵ value in our model represents how damaged cells have compromised recovery mechanisms. Connecting this to real cardiac tissue, this can reflect how scarred regions have disrupted ion pumps, with impaired calcium handling due to disrupted Ca^{2+} channels which refrains the tissue from returning to its resting state after excitation.

Effect of Decreasing β :

The v -nullcline is given by:

$$v = \frac{u + \beta}{\gamma}$$

Decreasing β :

- Shifts the v -nullcline downward in the phase plane, moving the intersection point of the nullclines (equilibrium point) downward.
- Reduces the excitation threshold needed to move the system away from equilibrium.

With a decreased threshold required for activation, spirals are much more likely to form in that region.

Biological Connection: In real hearts, fibrotic tissue demonstrates altered potassium channels and calcium handling proteins, creating localized regions that differ substantially from surrounding healthy tissue. The reduced potassium channel density alters the resting membrane potential and weakens the region by making it more easily triggered by smaller electrical signals.

Why not an altered γ parameter? γ primarily affects the recovery dynamics of the system. Changing γ does not have as much of an effect on representing the volatility of a scarred region as ϵ and β do.

Animation of Fibrosis:

These two altered parameters will be therefore used to mimic conditions like localized fibrosis or scarring from previous heart attacks, where the severity of damage is represented by the ϵ and β values chosen. Studies have shown that when the normal heart waves interact with these regions, disruptions can affect the system's overall dynamics, potentially forming spiral waves.

Thus, we can integrate the healthy heart waves that propagate from the top left sinoatrial node at a rate of 60 bpm, along with our low Ornstein-Uhlenbeck SDE parameters of ($\theta = 0.01$, $\sigma = 0.01$). Then, adding in the new ($\frac{points}{6} \times \frac{points}{6}$) sized damaged region, we can simulate this depiction of tissue variation below:

An Evolution of a Fibrotic Region Interacting with a Heartbeat Wave ($\theta = 0.01$, $\sigma = 0.01$)

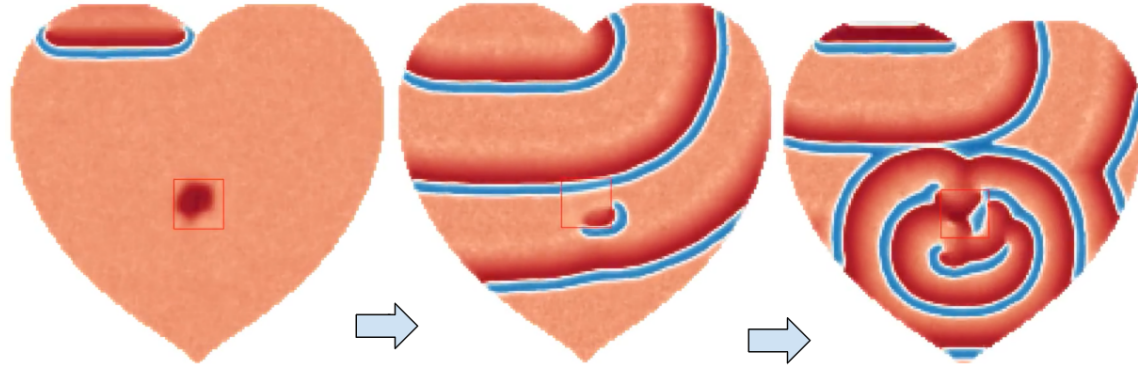


Figure 23: Evolution of the damaged region with low natural biological noise parameters ($\theta = 0.01$, $\sigma = 0.01$), and with altered Fitzhugh-Nagumo region parameters: ($\beta = 0.67$, $\epsilon = 0.27$), in 10 seconds of simulation time, with the normal heart's 60bpm time dimensionalization.

Animation: [Click Here](#): Notice the red square, indicating the border of the damaged region inside. As the normal heart waves propagate downward from the top left, with its increased electrical charge, when interacting with the affected region, causes a spiral perturbation to form, that eventually will overtake the entirety of the grid.

5.1 Varying the Region Size and Severity of Fibrosis Damage

The effects of fibrosis can be explored further by modifying both the size of the damaged region and the severity of the impairment. This includes decreasing the region's size and adjusting parameters to alter its impact.

Decreasing β and ϵ even more, this should make it even easier for perturbations to form, representing an even weaker region of the heart, but a smaller region could suppress potential spiral formation. We can also test varying the area of the damaged region to see if this changes the disruptive nature of the instability.

5.1.1 Concentrated High levels of Damage: Representing Automatic Foci

Automatic Foci, also known as ectopic pacemakers, are **small** abnormal regions in the heart that can spontaneously generate electrical impulses, independent of the sinoatrial node, the heart's primary pacemaker. When these ectopic sites become active, they can essentially create their own electric waves that pulsate outward, disrupting the normal heart rhythm. In a healthy heart, the sinoatrial node's powerful propagating waves will consistently suppress these potential pacemaker activities.

However, research has shown that in *especially* damaged fibrotic regions of cardiac tissue, the strength of these unwanted ectopic waves can be dramatically increased. Research by Campos et al. demonstrated that introducing non-conducting elements designed to mimic severe fibrotic damage in cardiac tissue models resulted in spontaneous ectopic beats with increased automaticity [21]. Their simulations showed

that the likelihood of this occurring depended heavily on both the severity and spatial distribution of the damaged regions.

Importantly, ectopic beats are *not* characterized by spirals. Instead a circular reentry pattern is more likely because the waves have a limited space to travel around, maintaining a closed-loop propagation

We can mathematically represent by lowering the values of β and ϵ further, to $(\beta = 0.62, \epsilon = 0.22)$. The designated size of the fibrotic region will be dramatically decreased as well. This will represent a small, yet incredibly damaged area of the heart, akin to modern research done on the phenomena.

Localized Severe Fibrotic Scarring: Automatic Foci

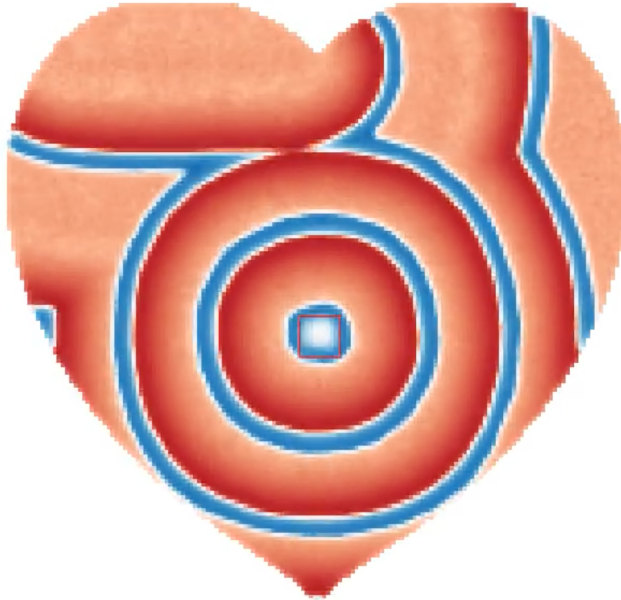


Figure 24: Severe fibrotic scarring in a region represented with $(\beta = 0.62, \epsilon = 0.22)$. As can see, the region systematically creates its own electrical waves that push back against the sinoatrial node.

Animation:[Click Here:](#)

5.2 Fibrotic Region Size Analysis:

Due to these propagations being inherently different from the classic spiral formations we have seen previously, we could propose a hypothesis: The size of the damaged region plays a critical role when determining if self-sustaining spiral waves could form from fibrotic scarring.

If a fibrotic region is too small, spirals are unlikely to form within it, as the oscillations have limited space to propagate, preventing the development of sustained, large-scale spiral waves. For wave propagation to occur in a smaller region, the severity of fibrotic damage must be extremely high. In contrast, a larger fibrotic region increases the likelihood of wave fragmentation, providing sufficient excitable tissue space around the core of a potential spiral to help facilitate its growth.

Research supports this, as specifically, studies have indicated when fibrosis covers a large area of

approximately 30–50% of the muscle tissue, the potential for arrhythmias such as tachycardia and fibrillation is at its peak. Any smaller or larger tissue size hinder spiral formation, as slow conduction may eventually transition to non-conduction in fibrotic tissue, preventing reentry circuits [7].

This differs from the dead cell model, where the affected region was completely non excitable as it essentially acting as a conduction block. In that case, we saw that *no matter what size the dead cell area was*, when a normal heart wave encountered the dead cell region at a specific angle, it could not propagate through, forcing it to bend and wrap around the obstacle, leading to at least one spiral wave formation omitting from the sharp corner(s).

In contrast, the fibrotic region here is still excitable, and it alters conduction velocity and wave dynamics. This means that rather than simply redirecting the wavefront as in the dead cell model, the fibrosis slows down conduction (based on its severity of damage), increasing it's electrical volatility, and enhances heterogeneity, making the conditions for spiral wave formation highly dependent on the region's size. Additionally, unlike completely dead tissue, fibrotic regions maintain some degree of ion transport capability, albeit with significantly altered electrolyte behavior.

Testing another size, we can see that mathematically with the Fitzhugh Nagumo model as by increasing the size of the region to $(\frac{points}{4} \times \frac{points}{4})$, we require less of an extreme change in β and ϵ , ($\beta = 0.68$, $\epsilon = 0.28$) to form not only perturbations, but spiral waves in the region (albeit much later in the simulation time).

Animation: [Click Here](#):

This shows that a region that is not as badly damaged can still create spirals if it is larger. However, these spirals could take a lot longer in the simulation to form, but it is worth noting that after 10 simulations of the $(\frac{points}{6} \times \frac{points}{6})$ region at ($\beta = 0.68$, $\epsilon = 0.28$), only one simulation generated spirals at all. This suggests a critical relationship between the region's size and the severity of damage.

Can we quantify the relationship between fibrotic damage parameters and spiral formation?

To address this, we'll answer two key questions.

- 1) Can we measure how the severity of fibrotic damage influences spiral formation time?
- 2) How does the size of the fibrotic region affect this relationship?

To answer these fundamental questions, we need a method that can systematically measure spiral formation and its respective time across parameter space.

6 Quantifying Vulnerability: MRT Spiral Formation Analysis of Fibroticity:

This section will first initially seek to provide a statistically robust framework for quantifying exactly when spiral waves emerge under varying conditions. By measuring the average time to first spiral formation across numerous iterations, insights into the vulnerability of fibrotic tissue could be revealed, potentially validating clinical trials.

6.1 MRT for Spiral Formation in Varying Sizes of Fibrotic Damage

The severity of damage will be represented by varying combinations of β and ϵ in the parameter space. Starting with the first key question, measuring severity, the size of the region will be varied later so for now we shall use $(\frac{points}{6} \times \frac{points}{6})$.

Given our integration of stochasticity into the fibrotic model, a single simulation per parameter set would be statistically inadequate. Since each stochastic simulation produces unique results (even with low constant noise parameters $\theta = 0.01$, $\sigma = 0.01$), we must run numerous automated trials for each (β, ϵ) combination to calculate reliable average spiral formation times across a parameter space.

Defining the Mean Response Time (MRT)

The Mean Response Time (MRT) will be used to measure the average time taken for a spiral to form in the region over a range of different β and ϵ parameter values.

$$MRT = \frac{1}{N} \sum_{i=1}^N T_i \quad (19)$$

Following the approach of Valenti et al, we analyze the Mean Response Time (MRT); however, we focus solely on measuring the time taken for the first spiral to occur, rather than including small non-spiral perturbations [4],[9]. Here,

- T_i represents the total time at which the first spiral takes to develop.
- N is the number of trials that will be run for each and every parameter combination. We will choose $N = 100$.

We now proceed on identifying true spiral formation.

6.1.1 Defining Spiral Wave Detection

Previously we looked at the method of using 3 probes to locate a potential spiral source, and then analyzed its period to verify if it was indeed a spiral. While that method involves a sense of realism, its drawbacks were apparent. Instead we will now iterate over every single point in the grid over every single time loop, to check if a spiral source is being formed. First, establishing crystal clear criteria for what a formed spiral looks like is crucial in order to analyze their formation times.

- A complete 360° rotation is observed
- The spiral tip follows a stable trajectory
- The wave maintains its shape for at least one full rotation, and is not destroyed.

Given that every single spiral wave formed in this system has the exact same period of the tachycardia spiral as seen in chapter 8 and 10, this simplifies things for us. Given the period is essentially the cycle length of the re-entrant spiral circuit, once a spiral forms, if the tip survives for a period of **572 milliseconds**, then we know it has completed one full rotation, and isn't merely some disorganized perturbation.

6.1.2 Spiral Tip Detection Algorithm

Rotational Density:

First, we calculate the rotational density $\rho(x, y)$ at each point:

$$\rho(x, y) = |\nabla u \times \nabla v|^2 \quad (20)$$

Where the gradient measures spatial rate of change in each direction, and the curl: $\nabla u \times \nabla v$ is used to measure local rotation strength. Combined together, this measures the local rotational strength at each grid point (x, y) . When this value is non-zero, it indicates potential spiral tip activity.

Tip Location

The center of rotation (spiral tip coordinates) is then calculated using weighted averages:

$$(x_{tip}, y_{tip}) = \left(\frac{\iint x \cdot \rho(x, y) dx dy}{\iint \rho(x, y) dx dy}, \frac{\iint y \cdot \rho(x, y) dx dy}{\iint \rho(x, y) dx dy} \right) \quad (21)$$

These integrals effectively compute the "center of mass" of the rotational activity, where $\rho(x, y)$ acts as a density function. The numerators weight each position by its rotational strength, while the denominators normalize the result.

Numerical Implementation

Since we're working with discrete grid points, the double integrals are approximated using the trapezoidal rule:

$$\iint \rho(x) dx dy \approx \sum_i \sum_j \frac{\Delta x \Delta y}{4} (\rho_{i,j} + \rho_{i+1,j} + \rho_{i,j+1} + \rho_{i+1,j+1}) \quad (22)$$

This converts the continuous integrals into a discrete sum suitable for numerical computation, where:

- $\Delta x, \Delta y$ are the grid spacings, with (i, j) index the grid points
- The average of four adjacent points provides a better approximation than single-point sampling

Iterating over the region at every single time loop, whenever a grid point has this property, we will time it by 572 milliseconds (9.53 time units), and if it is still non-zero, we flag it as a formed spiral in the MRT experiment. Then we add together the time duration prior to formation and 572 milliseconds of growth time for that specific combination of β and ϵ in a simulation N . There will be 160 units of simulation time (approx. 10 seconds).

Parameter Space:

Sampling the parameter space with 6 values each for β and ϵ from 0.69 to 0.64 and 0.3 to 0.24 respectively. Values lower than $\epsilon = 0.24$ and $\beta = 0.64$ yielded behavior characteristic of *Automatic Foci*, circular perturbations being systematically formed with no spiral formation, despite a larger fibrotic region size. Any higher values were the default Fitzhugh-Nagumo parameters $\epsilon = 0.3$ and $\beta = 0.7$ that would have made the purpose of the region irrelevant, and no spirals were formed at those values. Thus, the

partitioned values are below, giving $6 * 6 = 36$ different combinations, multiplied by $N = 100$ yields 3,600 total simulations.

$$\beta = \{0.69, 0.68, \dots, 0.65, 0.64\},$$

$$\epsilon = \{0.29, 0.28, \dots, 0.25, 0.24\}.$$

With 10 seconds of simulation time, we now have the means to generate an insightful heat map for varying epsilon and beta within the damaged region.

6.1.3 MRT Result and Heatmap:

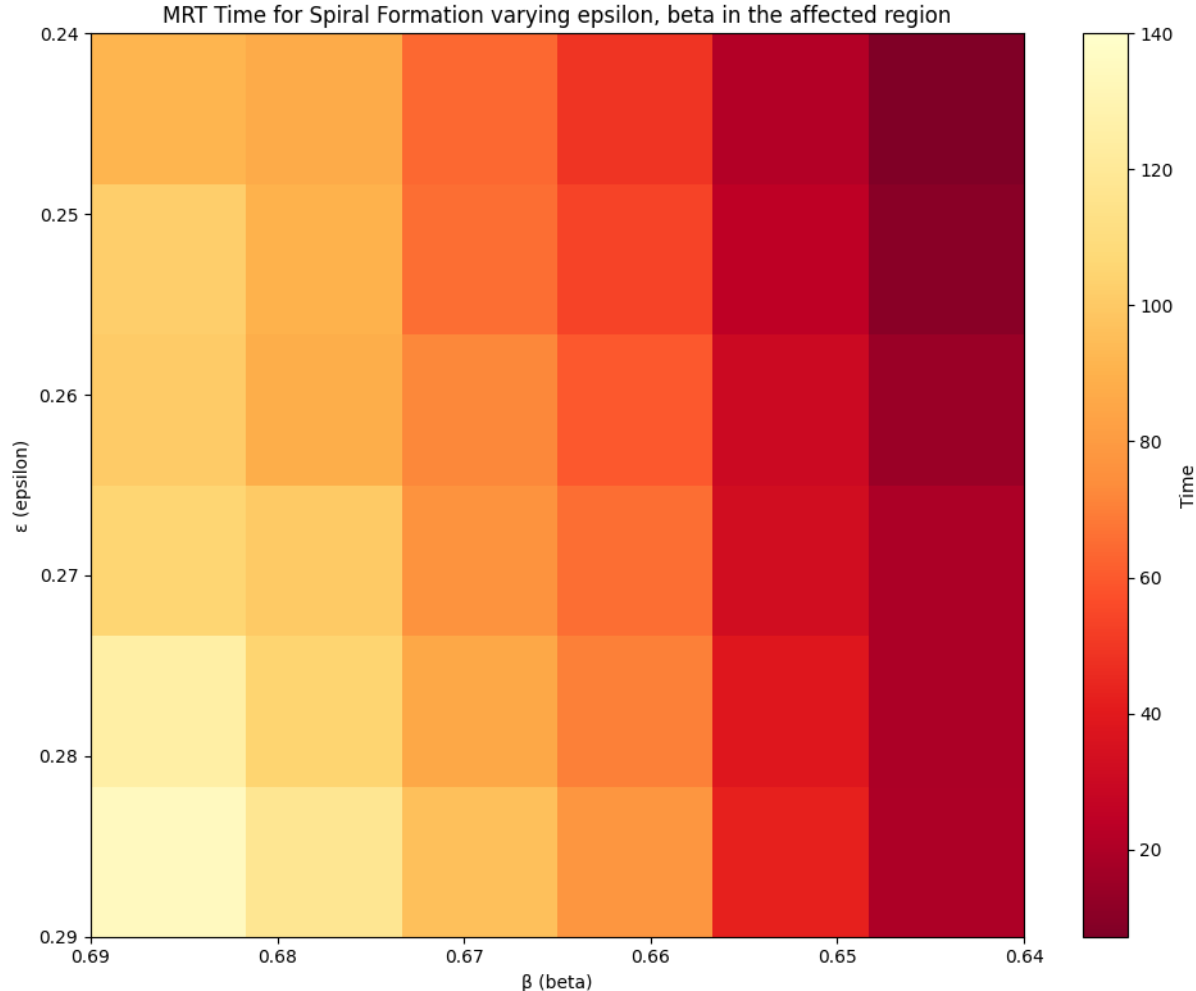


Figure 25: Spiral MRT heatmap across the ϵ and β parameter space.

Python Output

Results Summary:

Minimum MRT: 9.868 time units (0.59 sec) epsilon=0.24, beta=0.64

Maximum MRT: 138.315 time units (8.32 sec) epsilon=0.29, beta=0.69

Average MRT: 84.293 time units (5.07 sec)

With the lowest combination of ϵ (higher vulnerability) and β (decreased threshold for activation), this represents an incredibly damaged region of the heart, and we notice in the heatmap that the time it takes for a spiral to form is near instant, as the Minimum MRT time of 0.59 seconds (including the 0.57 seconds it takes to fully form once started).

For the Maximum MRT, the parameter combination which created spirals the slowest, is unsurprisingly, the parameter values closest to the default Fitzhugh Nagumo model, $\epsilon = 0.29$, and $\beta = 0.69$. It took 8.32 seconds to form the requirements for a spiral, 1.68 seconds away from the simulation time limit of 10 seconds.

The Average MRT time was 84.293 time units, or 5.07 seconds, and the parameter combination that was closest to this time was $\epsilon = 0.26$, and $\beta = 0.67$.

This ultimately shows that in the Fitzhugh Nagumo system, the more damaged a region is, (represented by a lower ϵ and β), the faster and easier it is to form a spiral.

Can we analyze which parameter has more jurisdiction over varying the system's time for first spiral formation?

6.1.4 Parameter Influence Analysis:

This heatmap exhibits an approximately linear variation along the diagonal, and is characterized by smooth, monotonic behavior without any abrupt jumps and nonlinearities. With this behavior, we can aim to quantify which parameter has greater influence on spiral formation time with a multiple linear regression model.

$$\text{MRT} = b_0 + b_1\epsilon + b_2\beta \quad (23)$$

Where: b_0 is the intercept, b_1 is the coefficient for ϵ , and b_2 is the coefficient for β . Before conducting the regression analysis, basic descriptive statistics for our parameters is required:

$$\mu_\epsilon = \frac{1}{n} \sum_{i=1}^n \epsilon_i, \quad \mu_\beta = \frac{1}{n} \sum_{i=1}^n \beta_i \quad (24)$$

Where μ_ϵ and μ_β are the means of the parameter values used in our simulations.

The standard deviations can be calculated as:

$$\sigma_\epsilon = \sqrt{\frac{1}{n} \sum_{i=1}^n (\epsilon_i - \mu_\epsilon)^2}, \quad \sigma_\beta = \sqrt{\frac{1}{n} \sum_{i=1}^n (\beta_i - \mu_\beta)^2} \quad (25)$$

A standardization of the parameters is required, in order to make the coefficients comparable despite different scales and units.

$$\epsilon_{\text{standardized}} = \frac{\epsilon - \mu_\epsilon}{\sigma_\epsilon}, \quad \beta_{\text{standardized}} = \frac{\beta - \mu_\beta}{\sigma_\beta} \quad (26)$$

This standardization transforms both parameters to have mean 0 and standard deviation 1, allowing direct comparison of their effects. Running the regression model using the standardized variables:

$$\text{MRT} = b_0 + b_1\epsilon_{\text{standardized}} + b_2\beta_{\text{standardized}} \quad (27)$$

The regression yielded the following standardized coefficients:

$b_1 = 0.31$ for $\epsilon_{standardized}$ and $b_2 = 0.78$ for $\beta_{standardized}$

These results indicate that a one standard deviation change in β results in a 0.78 standard deviation change in MRT, while a one standard deviation change in ϵ results in only a 0.31 standard deviation change in MRT. The ratio of these effects ($\frac{0.78}{0.31} \approx 2.5$) demonstrates that β has approximately 2.5 times more influence on spiral formation time than ϵ .

A coefficient test, using

$$R^2 = 1 - \frac{\text{Sum of Squared Residuals}}{\text{Total Sum of Squares}}$$

shows that this model, which includes an intercept, yields coefficient of determination (R^2) for the model is 0.83, indicating that 83% of the variation in spiral formation time is explained by variations in ϵ and β .

This mathematical finding aligns strongly with experimental observations that potassium concentration (which primarily affects activation threshold analogous to β) has greater influence on arrhythmia susceptibility than calcium handling abnormalities (relating to overall electrical dynamics represented by ϵ). Research conducted by the Rotterdam Study found that participants with hypokalemia had a higher risk of developing atrial fibrillation compared to those with normal potassium levels [25]. In contrast, while abnormalities in calcium levels can disrupt the heart and promote arrhythmias, a review in Frontiers in Physiology indicated that while significant, these mechanisms might not influence arrhythmia susceptibility as strongly as potassium concentration does [28].

6.2 MRT for Spiral Formation in Varying Sizes of Fibrotic Damage

Can we create a connection between size of the damaged fibrotic region and how long it takes for a spiral to form, if at all?

6.2.1 Biological Research on Fibrotic Size:

Research indicates that the extent of cardiac fibrosis significantly influences arrhythmia formation. Both experimental data and computer simulations suggest that fibrosis covering less than 20% or more than 80% of the myocardial area is relatively benign, whereas spiral formation potential is maximal at 30–50% fibrosis.

The counterintuitive nature of this phenomenon actually makes sense when you think about how spiral waves form and propagate. For a spiral wave to form and sustain itself, you need a large enough region of damaged tissue that can support the formation of the tip and enough healthy tissue around it to allow the wave to oscillate and complete its rotation.

When the damaged region is very small (less than 10%):

There isn't enough disrupted tissue to break up the normal wave patterns. Only non-spiral perturbations will occur *if it is damaged enough*, as seen in the "Automatic Foci" example from Chapter 11.

When the damaged region is very large (larger than 80%):

There isn't enough healthy tissue left and the tested grid points become essentially electrically inert, as the waves can't propagate properly to form spirals.

The study suggests that the preferred area for spiral formation (30-50%) provides enough damaged tissue to form spirals. This is why intermediate levels of damage are paradoxically more dangerous - they create the perfect conditions for sustaining arrhythmias. A heart that's 90% damaged might actually be less likely to form spirals because it lacks the infrastructure needed to maintain them, even though it would have other severe problems.

While these biological studies provide valuable insights, it's important to note that our FitzHugh-Nagumo simulation operates on a simplified 2D grid of 160×160 points, whereas real cardiac tissue is a complex 3D structure with millions of cells, heterogeneous patterns, and intricate fiber orientations.

Nevertheless, the FitzHugh-Nagumo model, even in this simplified form, can help us investigate whether it can handle this scientifically proven relationship between damaged region size and spiral formation. If our model demonstrates similar behavioral patterns, it would support the claim that this phenomenon emerges from the fundamental properties of wave propagation in excitable media, rather than strictly cardiac tissue.

6.3 Mathematical MRT Setup for Size Variation:

Testing every parameter combination for numerous different sizes, is a time-consuming process that would not be computationally feasible. Instead, we could select a few representative points in the parameter space that showed interesting behavior in our original analysis of region size ($\frac{points}{6} \times \frac{points}{6}$). Additionally, to further increase the size of the grid points, the heart mask border will be removed, replaced with the square edges from our original default spiral.

Since our previous findings indicated that β exerts a much stronger influence on spiral formation than ϵ , we prioritize varying β across the range $\beta = \{0.7, 0.69, \dots, 0.65, 0.64\}$ while adjusting ϵ accordingly. Testing these specific combinations across a range of fibrotic region sizes allows us to capture key size-dependent trends without excessive computational cost.

Parameter Space for the Fibrotic Region Size:

Will use Region Size = $\{10\%, 20\%, \dots, 70\%, 80\%\}$, and the low Ornstein-Uhlenbeck parameters to represent a realistic biological noise as before with ($\theta = 0.01$, $\sigma = 0.01$).

6.3.1 Spiral Formation Time V. Damaged Region Size Graph and Analysis

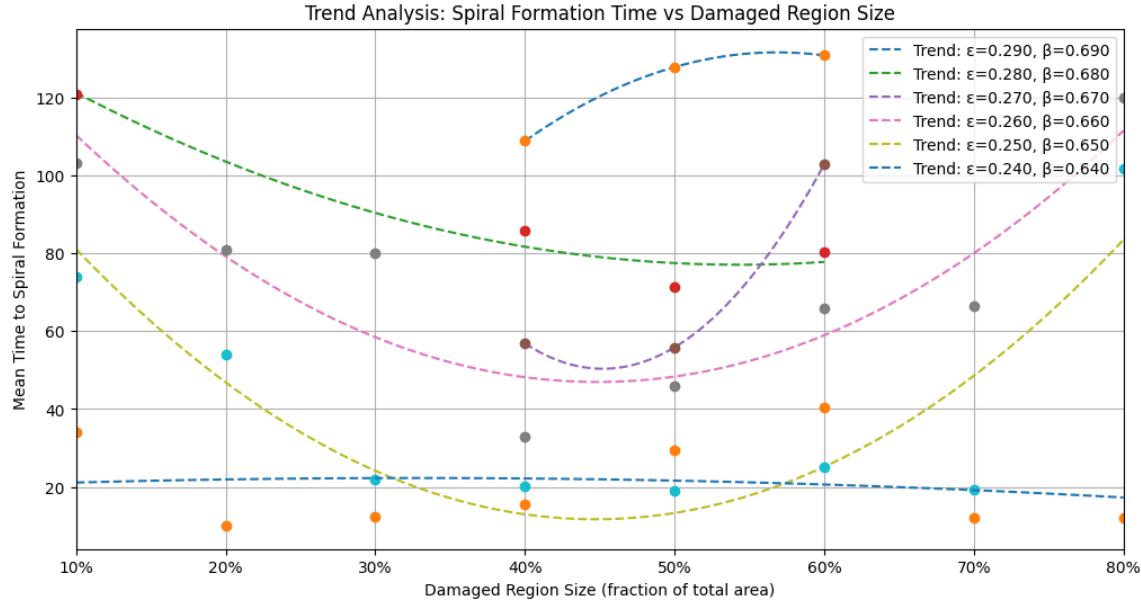


Figure 26: Trends over time of varied parameter combinations over different fibrotic region sizes.

Analysis:

The observed trends suggest that the mean response time (MRT) often follows a quadratic relationship with region size. Across most parameter sets, the minimum MRT occurs for fibrotic coverage between 30% and 60%, which aligns with existing research on arrhythmia formed from cardiac fibrosis. Notably:

- Parameter sets closer to the default values ($\epsilon = 0.3, \beta = 0.7$), fail to generate spirals in very small or very large damaged regions.
- As ϵ and β decrease down the parameter space, on average, the MRT trends start resemble quadratic curves, with intermediate region sizes yielding the fastest spiral formation.
- Very small fibrotic regions (ex. 20%) tend to delay spiral formation, due to insufficient structural heterogeneity as mentioned previously.
- Conversely, very large fibrotic regions (ex. 70%) also exhibit larger MRTs, due to excessive conduction block (majority of grid points electrically inert).

However, once we decrease ϵ and β far enough down the parameter space to $\epsilon = 0.24$ and $\beta = 0.64$, spirals will form almost immediately, regardless of region size. At 80% size, the simulation generates spirals near instantly as well. Animation: [Click Here](#): But for slightly higher parameters, ($\epsilon = 0.25, 0.26$ and $\beta = 0.65, 0.66$), the dependence on region size becomes more pronounced. We can see below that in an animation with 80% of the grid covered by a fibrotic region, despite with relatively sensitive parameters ($\epsilon = 0.26, \beta = 0.66$), it takes an exceptionally long time for a spiral to form, ($\tilde{7.5}$ seconds) into the animation. This differs to the smaller region we had in the ($\frac{points}{6} \times \frac{points}{6}$) sized animation, where $\epsilon = 0.26$ and $\beta = 0.66$ yielded an MRT time of 71.24 time steps ($\tilde{4.3}$ seconds).

80% Fibrotic Coverage of Grid

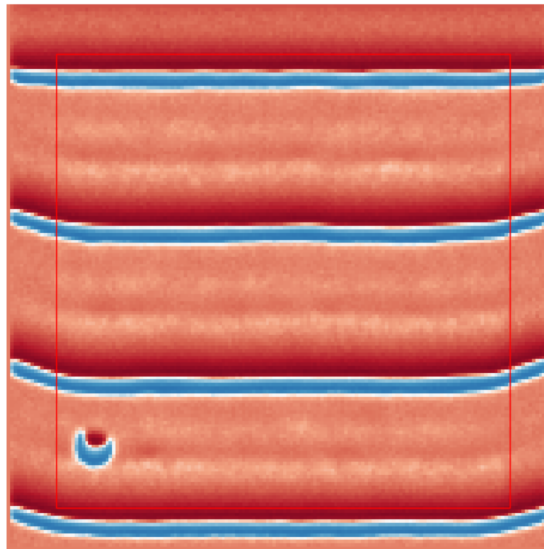


Figure 27: 80% of the grid covered with $\epsilon = 0.26$ and $\beta = 0.66$. See interior of red square for fibrotic region. This snapshot was taken near the end of the simulation, around 9 seconds.

Another simulation with those same parameters, but with a slightly longer run time, we get a similar animation: [Click Here](#):

6.3.2 Quadratic Trend Analysis

We can find the average percentage that had the minimum MRT time for each parameter combination (ϵ, β) tested here.

Fitting a quadratic function to the data using interpolation:

$$T(S) = aS^2 + bS + c \quad (28)$$

The minimum time to spiral formation occurs at $S_{\min} = -\frac{b}{2a}$, representing the optimal damaged region size.

where a, b, and c are coefficients obtained via quadratic interpolation using NumPy's `np.polyfit`.

```

1 # Find minimum point analytically
2 a, b, c = z
3 if a > 0: # Ensure we have a minimum MRT, not maximum
4     min_x = -b/(2*a)

```

We can generate further insights with the following Python results.

Python Output

```
OPTIMAL DAMAGE SIZE ANALYSIS
=====
Parameter Set | Optimal Size | Minimum Time
-----
 $\epsilon = 0.290, \beta = 0.690 | 40.0\% | 108.87$ 
 $\epsilon = 0.280, \beta = 0.680 | 54.4\% | 77.09$ 
 $\epsilon = 0.270, \beta = 0.670 | 45.2\% | 50.36$ 
 $\epsilon = 0.260, \beta = 0.660 | 44.8\% | 46.92$ 
 $\epsilon = 0.250, \beta = 0.650 | 44.7\% | 11.69$ 
 $\epsilon = 0.240, \beta = 0.640 | 20.0\% | 8.12$ 
```

6.3.3 A Conclusive Written Analysis of Spiral Formation Time and Damaged Region Size

Our analysis of spiral formation dynamics in fibrotic cardiac tissue reveals a nuanced relationship between parameter values, damaged region size, and Mean Response Time (MRT). The results demonstrate that both the severity of fibrotic damage (represented by decreased ϵ and β values) and the spatial extent of the damaged region significantly influence spiral wave formation. This trend presents itself as quadratic, creating a 'preferred' range of fibrotic sizes for arrhythmogenesis. In small fibrotic regions (below 20%), limited area constrains wave propagation and insufficient heterogeneity exists to create spiral formation in an ample time period, if at all. Most notably, our findings align with biological research showing that when the fibrotic coverage increases to 30-50%, this creates optimal conditions for arrhythmogenic spiral formation, with the lowest MRT values observed in this range across most parameter combinations. With excessively large fibrotic regions (above 70%), as seen previously, the reduced availability of healthy tissue again increases formation time as the waves lack sufficient excitable tissue to complete rotation circuits. As damage severity increases (having lower ϵ and β values), spirals form more rapidly, regardless of fibrotic region size, with β exerting approximately 2.5 times more influence than ϵ on formation time. This U-shaped response curve emerges naturally from two opposing factors that must be balanced: insufficient tissue heterogeneity at small sizes versus insufficient excitable substrate at large sizes.

The quadratic relationship between fibrotic tissue extent and potential spiral formation represents a fundamental biological principle: the balance between sufficient heterogeneity to initiate spirals and the severity of impairment.

These findings have significant implications for understanding the relationship between fibrosis extent and arrhythmia vulnerability, and demonstrate that the FitzHugh-Nagumo model can accurately represent these cardiac wave dynamics in its excitable medium.

7 Conclusion

Over sixty years since FitzHugh and Nagumo's pioneering work in the early 1960s on neural excitability, their simplified model has proven to be incredibly important for modeling and understanding cardiac dynamics. Through a deep analysis of both deterministic and stochastic processes, this project has helped connect and validate a biological representation of cardiac dynamics with our mathematical framework, the Fitzhugh-Nagumo equations. Beginning with fundamental ODE and PDE implementations, we first explored how these equations could effectively model both normal cardiac behavior and the emergence of potentially dangerous spiral waves. The dead cell model showed that abnormal non-exitable obstacles can form a wave-break in a healthy heartbeat wave, creating an environment suitable for spiral formation. We then utilized these deterministic factors to briefly examine potential treatment methods using probe detection of the spiral source via period analysis, and then compared the similar methodologies to real-world clinical techniques.

Next, the introduction of stochasticity through the Ornstein-Uhlenbeck process provided an advancement in our modeling approach. By bridging mathematics to specific electrolyte imbalances, particularly potassium, sodium, calcium, and magnesium fluctuations, a more biologically realistic model was created with low temporal levels of noise. Despite relinquishing our previous deterministic control over perturbation time and location, it was established that we could represent numerous cardiac diseases more accurately solely with statistical variability. Our period analysis further quantified how these spirals can significantly increase heart rate, with average periods decreasing from around 1000ms in normal conditions to approximately 570ms during *tachycardia* and an irregular 418ms in the harmful *ventricular fibrillation*. This realistic time dimensionalization connects our mathematical modeling directly to clinically observable cardiac phenomena.

With our aforementioned framework established, we could then further analyze another arrhythmia, Fibrosis. Fibrotic regions not only alter tissue excitability but create localized electrolyte environments that further promote wave instability. Varying both the severity of the damaged area (ϵ, β), and size of the region, this helped us understand the potential severity of this arrhythmia. First we kept the size of the fibrotic region constant, and varied (ϵ, β) across a parameter space, and measured the average time it took for a spiral to form in the region using MRT analysis and a spiral tip detection method. Next, using slight variations in (ϵ, β), we then sought out to vary the size of the region. The quadratic relationship observed between damaged region size and Mean Response Time (MRT) matched clinical observations that a coverage of (30-50%) creates optimal conditions for arrhythmias, further reinforcing the strength of the Fitzhugh-Nagumo equations. Future work could extend this analysis by implementing this framework in full 3D models with anatomically accurate fiber orientation to potentially expand upon clinically relevant data.

While our 2D modeling approach necessarily simplifies the complex 3D structure of the heart, the alignment of our findings with clinical observations suggests that despite these constraints, **fundamental wave propagation principles remain the same**. The consistent reproduction of empirically observed phenomena, from our aforementioned example of fibrosis analysis, to the characteristic periods of different cardiac diseases, further reinforces the FitzHugh-Nagumo framework as a remarkable tool for cardiac dynamics.

Acknowledgements:

I would like to express my sincerest gratitude to Paul Sutcliffe for his assistance on this report and supporting me throughout the project. Additional acknowledgments to my group members Trinity Bowler and Grace Cowdry.

References:

- [1] D. Amar, H. Zhang, S. Miodownik, A. H. Kadish, and P. H. Stone. Age-related changes of autonomic tone in healthy subjects. *Journal of the American College of Cardiology*, 38(3):608–616, 2001.
- [2] J. Hayano and M. Yamada. Aging reduces complexity of heart rate variability in healthy subjects. *Aging (Albany NY)*, 2(10):744–749, 2010.
- [3] M. C. Wijffels, C. J. Kirchhof, R. Dorland, and M. A. Allessie. Atrial fibrillation begets atrial fibrillation: A study in awake chronically instrumented goats. *Circulation*, 92(7):1954–1968, 1995.
- [4] D. Valenti, G. Augello, and G. Spagnolo. Dynamics of a FitzHugh-Nagumo system subjected to autocorrelated noise. *Physica A*, 65:443–451, 2008.
- [5] I. Uzelac, S. Iravanian, N. K. Bhatia, and F. H. Fenton. Spiral wave breakup: Ventricular tachycardia to ventricular fibrillation and self-termination. *The Heart Rhythm Journal*, 19(11):P1914–P1915, 2022.
- [6] C. E. Rubio-Mercedes, G. Lozada, and F. Ortegon Gallego. Spiral-generation mechanism in the two-dimensional FitzHugh-Nagumo system. *Ricerche di Matematica*, 73(9), 2022.
- [7] T. P. Nguyen, Z. Qu, and J. N. Weiss. Cardiac fibrosis and arrhythmogenesis: The road to repair is paved with perils. *Journal of Molecular and Cellular Cardiology*, 70:83–91, 2014.
- [8] C. Cartier. Analysis of the Ornstein-Uhlenbeck process in cardiac dynamics. *Applied Physics Studies*, 2024.
- [9] G. Augello, D. Valenti, and B. Spagnolo. Dynamics of a FitzHugh-Nagumo system driven by a periodic signal in the presence of colored noise. In *Complexity, Metastability, and Nonextensivity: An International Conference*, pages 185–189. American Institute of Physics, 2007
- [10] Y. Li and J. Duan. Asymptotic behavior of random FitzHugh-Nagumo systems driven by colored noise. *Discrete and Continuous Dynamical Systems - B*, 23(4):1689–1720, 2018.
- [11] A. Garfinkel, Y.-H. Kim, O. Voroshilovsky, Z. Qu, J. R. Kil, Preventing ventricular fibrillation by flattening cardiac restitution. *Proceedings of the National Academy of Sciences*, 97(11):6061–6066, 2000
- [12] A. Garfinkel, Y. Tintut, D. Petrasek, K. Boström, and L. L. Demer. Pattern formation by vascular mesenchymal cells. *Proceedings of the National Academy of Sciences*, 101(25):9247–9250, 2004.
- [13] A. Garfinkel, M. L. Spano, W. L. Ditto, and J. N. Weiss. Controlling cardiac chaos. *Science*, 257(5074):1230–1235, 1992.
- [14] S. Krishnamoorthi, L. E. Perotti, N. P. Borgstrom, O. A. Ajijola. Simulation methods and validation criteria for modeling cardiac ventricular electrophysiology, 2014.
- [15] M. Bär, R. G. Elías, and E. E. N. Macau. Nonlinear physics of electrical wave propagation in the heart: a review. *Reports on Progress in Physics*, 87(1):016601, 2024

- [16] F. H. Fenton and E. M. Cherry. Models of cardiac cell. Scholarpedia, 3(8):1868, 2008.
- [17] F. H. Fenton and E. M. Cherry. Computationally efficient options for modeling cardiac excitation: from ions to tissue. Journal of Theoretical Biology, 2008.
- [18] Wikipedia contributors. FitzHugh-Nagumo model, Electrolyte diagram, Wikipedia, The Free Encyclopedia.
- [19] S. Krishnamoorthi, L. E. Perotti, N. P. Borgstrom, and O. A. Ajijola. Simulation methods and validation criteria for modeling cardiac ventricular electrophysiology. Circulation: Arrhythmia and Electrophysiology, 9(12):e004409, 2016.
- [20] Cleveland Clinic. Ventricular fibrillation. Cleveland Clinic, 2024.
- [21] B. Campos, J. R. L. de Oliveira, E. M. Cherry, and F. H. Fenton. Ectopic beats arise from micro-reentries near infarct regions in simulations of a patient-specific heart model. *Frontiers in Physiology*, 9:1910, 2018.
- [22] Mr. Abigail Clarkson. An explanation of Cardiac Action Potentials. *Natalies Casebook*, 2019.
- [23] Georgia Tech Studies Spiral Waves for Heart Research. Youtube, 2015:
<https://www.youtube.com/watch?v=1IhGJjYw5BQ>
- [24] CHM Computer History Museum, Richard FitzHugh at the National Institute of Health, copyright 1996-2025.
- [25] M. E. Van Der Ende, B. Dekker, T. G. M. Vervoorn, A. Hofman, and B. H. Stricker. Serum potassium levels and the risk of atrial fibrillation: The Rotterdam Study. *European Heart Journal*, 34(17):1202–1208, 2013.
- [27] S. V. Pandit, R. B. Trayanova. Potassium channel mutations and cardiac arrhythmias: Insights from computational models. *Circulation: Arrhythmia and Electrophysiology*, 9(12):e004667, 2016.
- [28] X. L. Hove-Madsen, J. L. Llach, L. R. Bayes-Genis, and C. M. Cinca. Calcium handling abnormalities and arrhythmogenesis. *Frontiers in Physiology*, 6:16, 2015.
- [29] J. G. Murray. Mathematical Biology, Volume 1: An Introduction. *Springer-Verlag*, 2002.
- [30] J. G. Keener and J. Sneyd. Mathematical Physiology. *Springer-Verlag*, 1998.
- [31] A. V. Panfilov. Effects of heterogeneous diffusive coupling on arrhythmogenesis. Circulation: Arrhythmia and Electrophysiology, 3(3):280–287, 2010.
- [32] Stanford Health Care. Ventricular tachycardia (VT). Stanford Health Care.
- [33] J. M. Davidenko, A. M. Pertsov, R. Salomonsz, W. Baxter, and J. Jalife. Stationary and drifting spiral waves of excitation in isolated cardiac muscle. Nature, 355(6358):349–351, 1992.
- [34] S. A. Luther, F. H. Fenton, B. G. Kornreich, A. S. Squires, and J. M. Davidenko. Low-energy control of electrical turbulence in the heart. Nature, 475(7355):235–239, 2011.
- [35] T. Liu, F. Xiong, X.-Y. Qi, J. Xiao, L. Villeneuve, I. Abu-Taha, D. Dobrev, C. Huang, and S. Nattel. Altered calcium handling produces reentry-promoting action potential alternans in atrial fibrillation-remodeled hearts. JCI Insight, 5(2):e133754, 2020.
- [36] M. R. Pandit and S. Jalife. Rotors and the dynamics of cardiac fibrillation. Frontiers in Physiology, 12:782176, 2021. [37] R. A. Gray, A. M. Pertsov, and J. Jalife. Spatial and temporal organization during cardiac fibrillation. Entropy, 17(3):950–974, 2015.
- [37] J. M. Davidenko, A. M. Pertsov, R. Salomonsz, W. Baxter, and J. Jalife. Spiral waves of excitation underlie reentrant activity in isolated cardiac muscle. Circulation Research, 77(3):593–607, 1995.
- [38] G. Alrabghi, Y. Liu, W. Hu, J. C. Hancox, and H. Zhang. Human atrial fibrillation and genetic defects in transient outward currents: mechanistic insights from multi-scale computational models. Philosophical Transactions of the Royal Society B: Biological Sciences, 378(1879):20220166, 2023.